Estuarine, Coastal and Shelf Science

Pelagic forage fish distribution in a dynamic shelf ecosystem – thermal demands and zooplankton prey distribution

--Manuscript Draft--

Manuscript Number:	
Article Type:	Research Paper
Keywords:	predator avoidance; East Australian Current; fisheries acoustics; forage fish; thermal tolerance; Australia, New South Wales, Montague Island, 36.0°S to 36.5°S, 150°E to 150.4°E
Corresponding Author:	Matthew Holland University of New South Wales AUSTRALIA
First Author:	Matthew M Holland
Order of Authors:	Matthew M Holland
	Jason D Everett
	Martin J Cox
	Martina A Doblin
	Iain M Suthers
Abstract:	The fine-scale distribution of pelagic forage fish is shaped by competing factors as fish optimise foraging while avoiding predation. We investigated the distribution of forage fish in surface waters of a dynamic coastal environment during two spring seasons to examine their distribution in relation to environmental variables. Using a multi-frequency echosounder and a towed Laser Optical Plankton Counter (LOPC), we investigated the effects of bathymetry, temperature, chlorophyll a concentration and zooplankton biomass on forage fish density. Relationships between fish density and these variables were consistent between surveys, despite large differences in total acoustic energy attributed to fish. Fish density showed a strong positive relationship with bathymetry and water temperature, and no relationship with surface zooplankton biomass density or chlorophyll a. This mismatch between fish and zooplankton may be caused by differences in the way fish perceive the distribution of prey versus temperature. Despite large concentrations of zooplankton in surface waters near the coast, the topographic constraint of shallow water on fish vertical distribution may increase the risk of predation in this region. Seeking out warmer temperatures along the shelf break may also improve fish physiological performance when cooler spring temperatures are below their thermal optimum. Understanding the distribution of coastal forage fish may contribute to interpreting nearshore movements of their predators.
Suggested Reviewers:	Michael Kingsford michael.kingsford@jcu.edu.au
	Sean Tracey Sean.Tracey@utas.edu.au
	Simon Pittman simon.pittman@plymouth.ac.uk
	David Secor secor@umces.edu
Opposed Reviewers:	

Matthew Holland, PhD candidate,
University of New South Wales
Sydney NSW 2052
Australia

21 July 2020

Dear Editor,

I am pleased to submit our original research article entitled ‘Pelagic forage fish distribution in a dynamic shelf ecosystem – thermal demands and zooplankton prey distribution’ by myself, Jason Everett, Martin Cox, Martina Doblin and Iain Suthers, to be considered for publication in ECSS. In this manuscript, we examined patterns in the distribution of forage fish, their prey and environmental variables which affect their physiology by comparing between two springtime surveys of a dynamic temperate shelf ecosystem in south eastern Australia. Between surveys conducted one year apart we found consistencies in the way forage fish were distributed along gradients of bathymetry and temperature, with a strong affiliation for the shelf break. We have attributed our findings to behavioural thermoregulation and predator avoidance.

We believe that this manuscript is appropriate for publication in ECSS and would be of interest to your readership due to our focus on a continental shelf ecosystem and because it touches on several key ECSS themes, including ‘species distribution in relation to varying environments’ and ‘oceanic forcing of semi-enclosed and continental shelf water masses’. We explore coast-to-shelf patterns in the distribution of low to intermediate trophic level species and their responses to biotic and abiotic environmental factors in a dynamic continental shelf ecosystem. Readers would likely also be interested in our work because it highlights the power of using a well-instrumented blue-water research vessel in a relatively shallow coastal environment.

We posed the question: In a dynamic coastal ecosystem, are there inter-annual consistencies in the way forage fish are distributed with static and dynamic environmental variables? We used a multifrequency echosounder and a towed laser optical plankton counter to examine how forage fish distribution related to temperature, salinity, bathymetry, phytoplankton and zooplankton density. We found consistent positive relationships of forage fish density with bathymetry and temperature, and no relationship with the distribution of lower trophic levels. Despite dense concentrations of zooplankton along the coast, forage fish demonstrated affinity for the shelf edge. We concluded that shallow water imposes limitations to the vertical distribution of forage fish, which may increase their perceived predation risk and cause them to avoid coastal areas. Further, concentrations of warm water offshore likely attract forage fish during the early spring when overall temperatures are below their physiological thermal optimum. Given that western boundary currents, such as the East Australian Current, are strengthening under the influence of climate change, we expect an increase in current-driven upwelling which could displace forage fish further offshore as they attempt to remain within warmer water, further separating them from site-attached predators such as seals and penguins.

In terms of authorship, JE has contributed much of the conceptual ecological context, MC has contributed to the acoustic analysis and modelling, MD has contributed oceanographic expertise and led the voyage in 2016, IS worked on the big picture, participated in both voyages and led the voyage in 2017, and I (MH) participated in both voyages, conducted the analysis, wrote the original manuscript and integrated all feedback from co-authors. All co-authors have agreed to be listed and have approved

the submitted version of the manuscript. This manuscript is original research and has not been submitted elsewhere for publication. We have no conflicts of interest to disclose.

Thank you for your consideration!
Sincerely,

Matthew Holland, PhD candidate,
Evolution & Ecology Research Centre,
Department of Biological, Earth and
Environmental Sciences,
University of New South Wales

Highlights

- Southern New South Wales regularly experiences reversals in current direction
- Reversals cause alternation state between temperate and subtropical water masses
- The shelf break attracted more forage fish despite greater prey density near shore
- Forage fish associated with water masses with positive temperature anomaly

Pelagic forage fish distribution in a dynamic shelf ecosystem – thermal demands and zooplankton prey distribution

Matthew M Holland[a,b,*], Jason D Everett[a,b,c], Martin J Cox[d], Martina A Doblin[b,e], Iain M Suthers[a,b]

[a] Evolution and Ecology Research Centre, School of Biological, Earth and Environmental Sciences, University of New South Wales, Kensington, NSW 2052, Australia

[b] Sydney Institute of Marine Science, Mosman, NSW 2088, Australia

[c] Centre for Applications in Natural Resource Mathematics, The University of Queensland, St Lucia, 4067 Queensland, Australia

[d] Australian Antarctic Division, Channel Highway, Kingston, TAS 7050, Australia

[e] Climate Change Cluster, University of Technology Sydney, Ultimo, NSW 2007, Australia

Target journal: Estuarine, Coastal and Shelf Science

Version 14 – 21 July 2020

Corresponding author:
Matthew M. Holland - m.holland@unsw.edu.au
Level 4, Biological Sciences South (E26), UNSW
Kensington NSW 2052
Australia

Conflict of interest statement: We have no conflicts of interest to declare

ABSTRACT

The fine-scale distribution of pelagic forage fish is shaped by competing factors as fish optimise foraging while avoiding predation. We investigated the distribution of forage fish in surface waters of a dynamic coastal environment during two spring seasons to examine their distribution in relation to environmental variables. Using a multi-frequency echosounder and a towed Laser Optical Plankton Counter (LOPC), we investigated the effects of bathymetry, temperature, chlorophyll *a* concentration and zooplankton biomass on forage fish density. Relationships between fish density and these variables were consistent between surveys, despite large differences in total acoustic energy attributed to fish. Fish density showed a strong positive relationship with bathymetry and water temperature, and no relationship with surface zooplankton biomass density or chlorophyll *a*. This mismatch between fish and zooplankton may be caused by differences in the way fish perceive the distribution of prey versus temperature. Despite large concentrations of zooplankton in surface waters near the coast, the topographic constraint of shallow water on fish vertical distribution may increase the risk of predation in this region. Seeking out warmer temperatures along the shelf break may also improve fish physiological performance when cooler spring temperatures are below their thermal optimum. Understanding the distribution of coastal forage fish may contribute to interpreting nearshore movements of their predators.

Keywords: predator avoidance; East Australian Current; fisheries acoustics; forage fish; thermal tolerance; Australia, New South Wales, Montague Island, 36.0°S to 36.5°S, 150°E to 150.4°E

1. INTRODUCTION

Continental shelf ecosystems form some of the world's most productive waters, often due to the upwelling of nutrient-rich bottom water caused by boundary currents, particularly in areas with a narrow continental shelf (Lucas et al. 2011). These productive waters not only support the majority of fisheries landings (Watson et al. 2004, Pauly et al. 2005), but also marine predators through the planktonic food web, from phytoplankton to zooplankton to pelagic zooplanktivorous fish, commonly referred to as small pelagic fish or forage fish (Pikitch et al. 2014). As a group, forage fish (e.g. herring, sardines, anchovies, mackerel) are some of the most abundant fishes in the world's oceans and are an essential link in the provision of energy to higher trophic levels (Bakun 2006, Pikitch et al. 2012).

Over broad geographic scales we know that the distribution of forage fish is highly variable (Holland et al. 2020), but generally should peak in biomass in temperate regions (Sala et al. 2012, Holmes et al. 2013, Longo et al. 2019, Holland et al. 2020). However, we do not currently know about the finer scale patterns of their distribution in coastal environments. There is evidence however, to suggest they are constrained by bathymetry (Maravelias 1999), temperature (Sato et al. 2018) and the distribution of their zooplankton prey (Ayón et al. 2008). In offshore environments, forage fish distributions are driven by the dynamics of oceanographic and ecological conditions of temperature, fronts and prey density (McInnes et al. 2017, Sato et al. 2018). In contrast, shallow coastal environments constrain the vertical distribution of forage fish around static spatial features (e.g. reefs) and therefore consistent patterns in distribution may emerge (Maravelias 1999).

Of particular importance for fish distribution is water temperature. The metabolic rates of fish impose a physiological requirement to seek out water masses within their thermal niche (Pribyl et al. 2016). Oceanographic fronts can present temperature boundaries to fish

distribution and may cause a mismatch between forage fish and their prey (Sato et al. 2018). These thermal barriers to distribution may be particularly prevalent in early spring, when water temperatures are generally at their annual minimum and fish actively migrate to remain on the warmer, offshore side of these fronts (Sato et al. 2018). In comparison, the distribution of zooplankton prey of forage fish is driven by passive processes of accumulation (Genin 2004, Aarflot et al. 2019) and the availability of phytoplankton (Benoit-Bird and McManus 2012). In coastal environments, these accumulations are generally caused by a combination of currents and topographic constraints on vertical migration (Genin 2004). Shallow topographies, such as in nearshore environments, present a barrier to the pre-dawn descent of zooplankton, resulting in their accumulation in surface waters after they are advected onto the shelf at night (Aarflot et al. 2019). Aarflot et al. (2019) proposed that these 'topographically constrained' zooplankton distributions likely have an important influence on forage fish.

For forage fish in coastal environments, the ability to locate the densest zooplankton aggregations would result in optimal foraging under ideal free distribution (IFD) theory (Tregenza 1995, Matsumura et al. 2010). However, fish only acquire limited information from their immediate surroundings and therefore some resources distributed along large-scale environmental gradients, such as temperature, should be easier for fish to navigate than more patchily distributed resources such as prey.

To explore the effects of these potentially competing drivers of thermoregulation and access to high-density prey aggregations on the distribution of forage fish, we examined the coastal waters off southeastern Australia, a part of the Great Southern Reef (Bennett et al. 2016). This area hosts a combined purse seine and midwater trawl fishery (Marton and Steven 2019) for yellowtail scad (*Trachurus novaezelandiae*), jack mackerel (*Trachurus declivis*), blue mackerel (*Scomber australasicus*) and redbait (*Emmelichthys nitidus*), with the greatest catch occurring in early summer (Stewart and Ferrell 2001). The inshore area of this region, in the

vicinity of Montague Island (36.251°S, 150.227°E), is home to year round populations of predators that feed on pelagic forage fish, including Australian and New Zealand fur seals (*Arctocephalus pusillus doriferus* and *Arctocephalus forsteri*, respectively) (Shaughnessy et al. 2001) and little penguins (*Eudyptula minor*) (Carroll et al. 2016). The narrow continental shelf here is only ~20 km wide, enabling large scale eddies formed by the East Australia Current (EAC) to encroach onto the shelf. Unlike areas to the north, the EAC eddy field (Everett et al. 2012) facilitates alternating influences of EAC and Tasman Sea water, making this location particularly dynamic. We expected both static (bathymetry) and dynamic (temperature, chlorophyll *a*, zooplankton density) drivers would influence the distribution of forage fish in coastal areas in relation to IFD theory (Fig. 1).

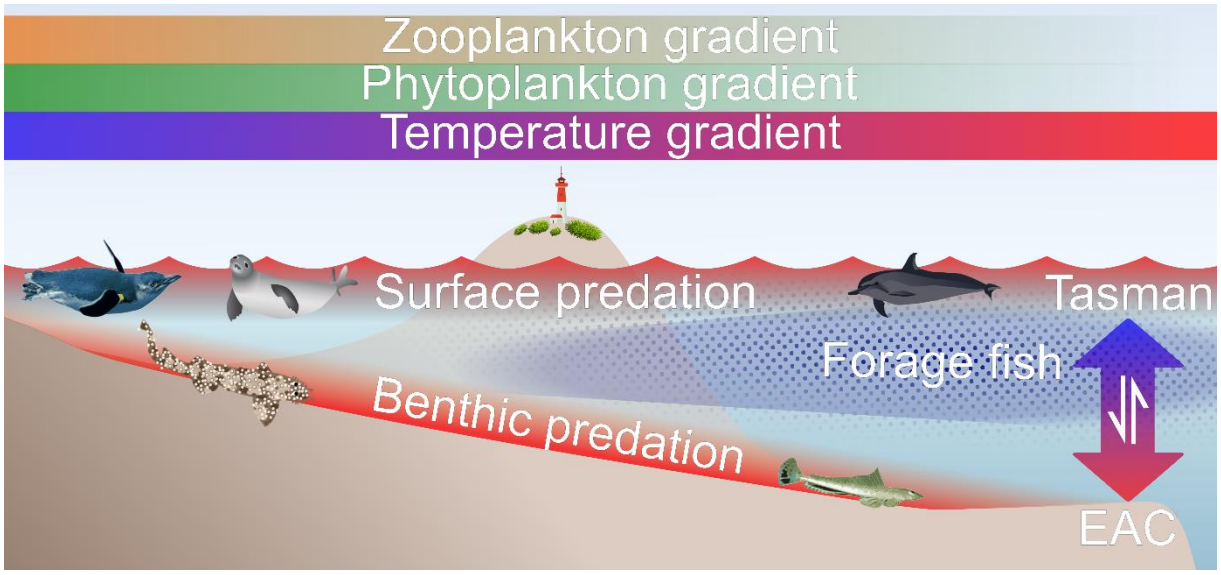

Fig. 1. Graphical abstract outlining the distribution of forage fish relative to horizontal gradients in zooplankton and phytoplankton, bathymetry and temperature and vertical gradients of predation pressure from the surface and the seafloor. The alternating influence of the EAC and the Tasman Sea is also indicated on right.

Our aims were to (1) examine whether the magnitude and the direction of associations was consistent when sampling in the same season in successive years; (2) examine static bathymetric influence on the fine-scale (10s of kms) distribution of fish which could drive persistent distribution; (3) examine the dynamic distribution of forage fish and compare their

distribution to temperature and their zooplankton prey; and (4) contextualise our surveys with long-term data on the dynamics of the East Australian Current.

2. MATERIALS & METHODS

2.1. Field surveys

Data was collected on two oceanographic voyages aboard the Australian research vessel, *RV Investigator* on 10 September 2016 and 17 September 2017, hereafter referred to as the 2016 and 2017 surveys. A series of six near-parallel ~15 km along-shelf acoustic transects (215 km total for 2016 and 145 km for 2017) were conducted at an average speed of 4.5 m s^{-1} both north and south of Montague Island, New South Wales (36.25° S, 150.22° E), which were planned to roughly follow the 30, 100 and 130 m isobaths (Fig. 2). For safety in nearshore waters, both surveys were conducted during daylight and transects were oriented parallel to the shoreline due to the risks of navigating a large (94 m) vessel with towed gear nearshore.

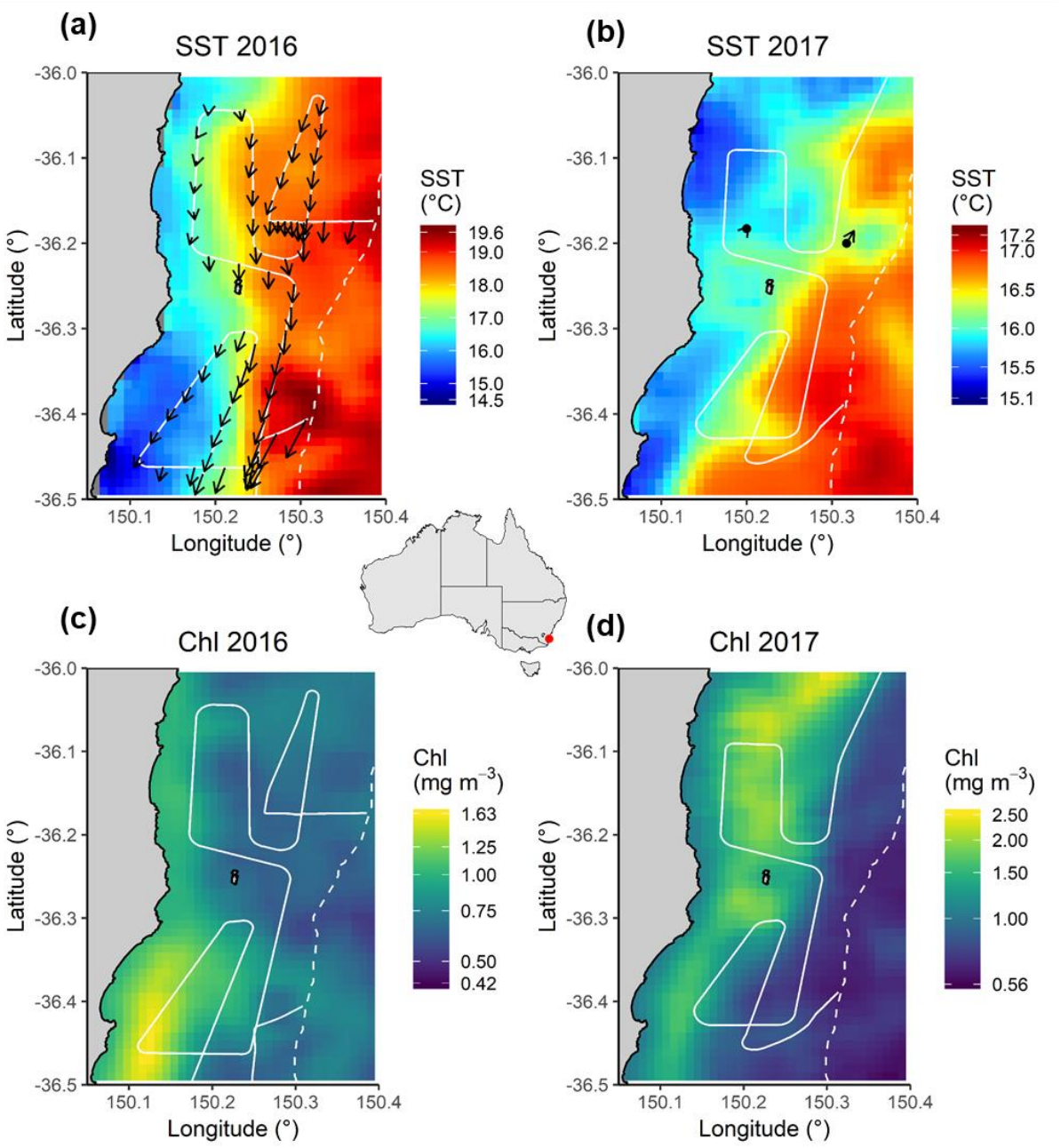

Fig. 2. Chart of ship tracks (solid white line) of acoustic surveys in 2016 (a) and (c), and 2017 (b) and (d). Vectors extending from the ship track (a) and from two fixed mooring locations (b) represent the current speed and direction between 20-30 m depth over a one-hour period, as measured by acoustic doppler current profilers (ADCP). The dashed white line represents the 200 m isobath. Background data for each plot represents 1 km resolution MODIS (Integrated Marine Observing System 2018) sea surface temperature (a) and (b) and chlorophyll *a* (c) and (d) averaged over a period extending six-days prior to each survey and smoothed using a focal mean around each pixel. Red dot on inset map (centre) included for approximate location. Note that each panel has an independent colour scale.

2.2. Acoustic data collection and processing

Acoustic data was collected concurrently using the RV Investigator's built-in Simrad EK60 (Kongsberg Maritime AS, Horten, Norway) multi-frequency echo sounder which pinged simultaneously at 18, 38, 70, 120, 200 and 333 kHz. Transducers were mounted ~6.4 m below the waterline on a lowered drop-keel. During the 2017 survey, the 120 kHz transducer was switched off due to interference with another sounder (data not shown; Table 1). The ship's acoustic doppler current profiler (ADCP) was active during the 2016 survey, however it was malfunctioning during the 2017 survey, so fixed mooring data was used instead to determine current bearing and velocity. This fixed mooring data was unavailable for the 2016 survey (Table 1).

Table 1. Summary of survey characteristics and instruments on both surveys. In this case, x indicates that data was available for the corresponding dataset, survey year combination, while - indicates the data was not available.

	2016	2017
Date	10 Sept 2016	17 Sept 2017
Local Time Start	04:51	05:25
Local Time Finish	20:39	17:52
EK60 18, 38, 70, 200, 333 kHz	x	x
EK60 120 kHz	x	-
Underway logging of temperature, salinity, chlorophyll *a* fluorescence	x	x
ADCP	x	-
Oceanographic mooring	-	x
Triaxus with LOPC	-	x

From fisheries logbook data for the months of August to October in the Montague Island region, *T. declivis* (jack mackerel) and *S. australasicus* (blue mackerel) contributed on average 74% and 19%, respectively, of the total catch by weight in Commonwealth Small

Pelagic Fishery for 2016 to 2019 (n = 67), inclusive of bycatch and discards (Supplement Fig. 1). Thus, it is most likely that the acoustic echoes classified as 'fish' (see below) in both surveys predominately belonged to these two species.

Acoustic data was processed using Echoview v8 (Echoview Software Pty Ltd, Hobart, Australia). Acoustic data was divided into a grid of cells 30 pings long by 10 m deep and integrated (McKelvey and Wilson 2006). Given a mean ship speed of 4.5 m s^{-1}, this resulted in grid cells approximately 150 m long. All subsequent processing was conducted with R v3.5.0 (R Core Team 2018). Grid cells were classified according to relative frequency response, as in Korneliussen and Ona (2002) (Supplement Fig. 2). Details and validation of methods employed to identify cells containing fish are outlined in Supplement, Classification methods.

Once grid cells were classified as either 'fish' or 'not fish', the values of the nautical area scattering coefficient (NASC), in units of m^2 nmi^{-2} (nmi = nautical mile; MacLennan et al. 2002), for the 38 kHz band were summed across each vertical section of water column for each cell classified as 'fish' down to a water depth of 30 m. Cells within this range that were not classified as 'fish' were assigned a value of zero. NASC (s_A) is represented here by the following equation from MacLennan et al. (2002):

$$s_A = 4\pi(1852)^2 s_a$$

Where s_a represents the area backscattering coefficient (m^2 m^{-2}) of a volume of water. This method provided a proxy for the relative density of fish in the surface waters along the ship track which could then be compared to the LOPC and underway measurements of environmental variables. The resulting classifications, using an identical method for both surveys, resulted in consistent mean relative frequency responses for fish across both surveys (Supplement Fig. 3).

2.3. Comparing fish distribution between surveys

To compare the distribution of surface forage fish between surveys (Aim 1), the region was divided into 12 polygons around the island to test for spatial differences in mean NASC using one-way ANOVA. The number of replicates used to calculate mean values for each polygon was also determined (Supplement Table 1). Polygons were generated by extending the coastline into three 0.065° longitudinal bands divided into four 0.1125° latitudinal blocks, centred at Montague Island at 36.25° S. These polygons were also bounded to the east by the 200 m isobath to exclude data collected off the continental shelf. The area of each polygon was approximately 70 km^2, encompassing a total area of 840 km^2.

To compare the raw acoustic classifications between surveys with finer detail (Aim 1), sample coordinates for both years were projected as UTM Zone 56 South so that a specific distance radius could be set for point matching between both surveys. Coordinates for the 2017 survey were matched to 2016 survey points using a 500 m search radius around each point and nearest neighbour search with the 'nn2' function in the R package RANN (Arya et al. 2017). Points were only matched to one nearest neighbour and if there were no corresponding points within the search radius, the point was excluded.

2.4. Measuring the distribution of zooplankton biomass

During the 2017 survey only, a Laser Optical Plankton Counter (LOPC) mounted on a towed-body Triaxus (MacArtney A/S, Esbjerg, Denmark) was towed at 4.5 m s^{-1} ~250 m behind the vessel at a depth of 20 m for the transects south of Montague Island. For the second half of this survey (the transects north of the island) the Triaxus was undulated (15-80 m depth) to examine vertical structure (Supplement Fig. 4). To ensure the data collected north and south of the island was comparable, we only extracted readings for the northern part of the survey between 15 to 25 m water depth.

Data from the LOPC from the 2017 survey was divided (binned) into size categories based on the equivalent spherical diameter (ESD) of measured particles and was then converted to biomass density (mg m^{-3}) assuming the density of water and the volume of water sampled (Suthers et al. 2006). The particles able to be accurately recorded by the LOPC ranged in size from 100 to 10,000 μm ESD. A previous analysis of gut-contents of some common forage fish in the region determined that the lower size limit of the prey they consumed was approximately 250 μm (Schilling 2014). Therefore, all particles smaller than 250 μm ESD (~1% of total biomass) were excluded from our analyses.

2.5. Bathymetry as a driver of fish and zooplankton vertical distribution

The vertical distribution of zooplankton biomass was examined across three levels of bottom depth (three isobaths) to determine whether the horizontal distribution of zooplankton at the surface was constrained by topography (Aarflot et al. 2019). A similar approach was also taken with fish NASC as well as temperature, by plotting their relationship with water depth for the same three isobaths (as a steeper decline in biomass with depth offshore versus along the coast would be evidence of such an influence). These isobaths corresponded to the three transects conducted north of Montague Island in 2017, where the towed body Triaxus was undulated through the water column and thus LOPC and temperature data were collected over a range of depths (15 to 80 m). These relationships were compared statistically using a GLM with gamma distribution (link = log) and analysis of covariance (ANCOVA). An interaction factor for 'isobath' was included and comparisons were conducted with Tukey's post-hoc tests.

2.6. Measuring in situ oceanographic variables

In situ temperature, salinity, chlorophyll *a* (Chl-*a*) concentration and bathymetry were examined as potentially important environmental variables affecting the distribution of fish and zooplankton. For modelling the distribution of fish, these variables were generated from

the ship's underway instruments which continuously sampled seawater from the 5 m depth drop keel. Bathymetry values were obtained from the ship's EK60 echosounder. Temperature and salinity were gathered by the ship's thermosalinograph and matched to acoustic data by 1-minute sampling intervals. Chl-*a* concentration was calculated from the ship's underway fluorometer using linear regression. The details of this approach are described in Supplement, Chlorophyll *a* methods.

For zooplankton distribution models, the towed-body Triaxus had built-in sensors which recorded temperature, salinity, and derived Chl-*a* from a calibrated Chl-*a* fluorometer and this data was integrated into 2-second intervals. For the Triaxus only, bathymetry was offset using trigonometric calculations based on the length of cable out and the pressure sensor on the Triaxus.

2.7. Establishing long-term oceanographic and fishery context

Montague Island is located south of the EAC separation zone (Cetina-Heredia et al. 2014) and is characterised by dynamic eddies (Everett et al. 2012). To contextualise the high temporal variability in oceanographic conditions for the study region (Aim 4), we examined MODIS Level 3 satellite altimetry, sea surface temperature and chlorophyll *a* (Chl-*a*) concentration data from IMOS (Integrated Marine Observing System 2018) for the date range September 2011 to February 2020. Using grid cells along the continental shelf edge only, we calculated monthly mean velocity vectors relative to the coastline angle. We also calculated temperature anomaly relative to climatological monthly mean from this date range, and the along-shelf current velocity within the southeast Australian coast (27.8 to 37.8 °S). We constructed a linear model with monthly mean values as replicates to determine whether variability in water temperature was driven by current direction at this location. Additionally, we modelled monthly mean Chl-*a* concentration by temperature to examine the influence of colder Tasman Sea water on phytoplankton biomass.

To establish the distribution of water temperatures in which *T. declivis* and *S. australasicus* were caught in the Commonwealth Small Pelagic Fishery, we extracted satellite sea surface temperature for the date and location of midwater trawls across a one-degree latitude band centred on Montague Island, occurring between August and October. We then compared the temperature in which *T. declivis* and *S. australasicus* were caught with the mean regional temperature between the 100 and 200 m isobaths, as fishing operations were concentrated around the 150 m isobath (149 ± 2.7 m). We also calculated the mean (weighted by catch per unit effort (CPUE) in kg hour^{-1}) temperature difference between fishing operations and regional mean temperature and conducted one-sample t-tests to determine whether this difference significantly differed from zero. This was intended to establish whether successful fishing operations were associated with temperature anomalies.

2.8. Modelling and predicting fish and zooplankton surface distribution

2.8.1. Modelling fish distribution along vessel track

To examine the effects of bathymetry on the distribution of fish during the ship surveys (Aim 2), two independent generalised linear models (GLMs) were created using surface NASC (summed NASC for cells classified as fish, <30 m deep) as the response variable for each of the two surveys. Both models used a single predictor, 'bathymetry'. A gamma distribution was used due to the zero-inflation of the response and strong right-skewness of the error distribution. In order to eliminate zeros to meet the requirements of a gamma distribution, a value equivalent to half the minimum non-zero value in the response was added to all response values (Johnson et al. 1970). Residual and response plots were scrutinised to ensure the GLMs did not violate model assumptions. The initial model structure (identical for both surveys) was (in script notation): *NASC ~ bathymetry*.

Two full models were then created using the additional predictor variables of modelled Chl-*a* and underway water temperature (Aim 3). Salinity data was available but not included as a predictor due to strong collinearity (correlation coefficient: >0.95 in 2016) with temperature. Both models were then subject to forward-stepwise Akaike information criterion (AIC) based selection. The full model structure (identical for both surveys) was as follows (in script notation): *NASC ~ bathymetry + temperature + log10(Chl-a).*

The resulting 2017 model was then combined with an additional predictor of zooplankton biomass to examine its effect on fish distribution. AIC was used to assess this model. This step was only performed on the 2017 data as the LOPC was not deployed during the 2016 survey (Table 1).

2.8.2. Modelling zooplankton distribution along vessel track

An additional zooplankton biomass model was generated for the 2017 survey to predict the distribution of zooplankton in the region, using the following initial predictors and was subject to the same forward-stepwise variable selection process as described above: *Zooplankton Biomass ~ log_10 (Chl-a) + bathymetry + temperatur*e.

2.8.3. Model inference and predicting continuous surface distribution from satellite data

All fish and zooplankton models were assessed for the presence of serial autocorrelation using the autocorrelation function and predictor test statistics were updated to incorporate heteroskedasticity and autocorrelation consistent (HAC) estimates using the sandwich package (Zeileis 2006). Thus, our adjusted inference takes autocorrelation into account and reduces the possibility of Type I errors.

Model predictions for NASC were generated from the final parsimonious NASC models for each survey. To generate continuous two-dimensional predictions across our study area, we used gridded satellite and bathymetry data. Predictions were conducted using 1 km resolution

MODIS satellite sea surface temperature and Chl-*a* averaged over a six day period prior to each survey to eliminate cloud cover (Integrated Marine Observing System 2018). MODIS data were smoothed using a focal function which calculates a mean value for the 24 pixels surrounding each pixel. For continuous bathymetry, 9 arc second bathymetry data from Geoscience Australia was used (Whiteway 2009). The same method was applied to predict the distribution of zooplankton at the time of the 2017 survey.

2.9. Comparing fish and zooplankton predicted surface distribution

To examine differences among two-dimensional continuous predictions for NASC among surveys, model responses were scaled from 0 to 1 by dividing by the maximum predicted value for each survey. The absolute difference between the 2016 and 2017 values were then calculated and plotted spatially. Similarly, predictions from the zooplankton distribution model were scaled to have a mean of 0 and a standard deviation of 1 along with the predictions of fish NASC for 2017 to examine differences in the distribution of fish and zooplankton. The difference between these two distributions was calculated and constrained to fall between -1 and 1, with negative values indicating a greater proportional density of zooplankton versus fish and positive values indicating the opposite.

3. RESULTS

3.1. Survey and long-term oceanographic conditions

The two surveys happened to sample two different oceanographic regimes (Fig. 2), characterised by a southward current in 2016, and a northward current in 2017. In 2016, a large warm core eddy of the East Australian Current (EAC) pushed currents southwards at a mean velocity of 0.6 m s^{-1} and bearing of 189° (as measured by the ship's 150 kHz ADCP), with mean water temperature (± SE) of 18.02 (± 0.02)°C and salinity (in PSU) of 35.62 (± 0.003). In contrast, during the 2017 survey, a large cold-core cyclonic eddy east of the island

generated a NNE flow past the study-site, with a mean velocity of 0.5 m s^{-1} and bearing of 25° (calculated from the 120 m depth mooring averaged over the duration of the survey) and a mean temperature (± SE) of 15.81 (± 0.02)°C and salinity of 35.64 ± (0.001).

During the 2016 survey a frontal edge between water masses was apparent from the southern extension of the EAC pushing warmer water along the edge of the shelf, whereas in 2017 there was a decreasing gradient in temperature from offshore to onshore and temperatures were less variable throughout the region, although colder overall (Fig. 2).

Ship-derived Chl-*a* (± SE) averaged 1.41 (± 0.02) in 2016 and 1.96 (± 0.04) in 2017 across the domain surveyed. Chl-*a* was significantly higher in 2017 (coef. = 0.52, $p < 0.0001$). In both years, Chl-*a* concentration increased in the cooler coastal side of the temperature front (Fig. 2). In the 2017 survey, Chl-*a* distribution was patchier throughout the survey region in comparison to 2016 (2016: CV = 53.2, 2017: CV = 83.1).

To place these two surveys in context, the long-term (8 year) oceanographic data for the shelf break indicated that Montague Island experiences net zero along-shelf current velocity, with an overall mean (± SE) of only 0.02 ± 0.01 m s^{-1} (Fig. 3a). This differed greatly from the coastline to the north, which experienced strong net southward flow of up to 0.47 m s^{-1}. However, despite net zero velocity, along-shelf currents around Montague Island reversed net directionality on average 3.6 times per year and monthly mean current ranged from -0.36 to 0.30 m s^{-1} (Fig. 3b). In agreement with ADCP data, current data from satellite altimetry indicated that the 2016 survey was conducted at a time with weak southward current (-0.04 ± 0.02 m s^{-1}) and the 2017 survey was conducted during moderate northward current (0.18 ± 0.02 m s^{-1}).

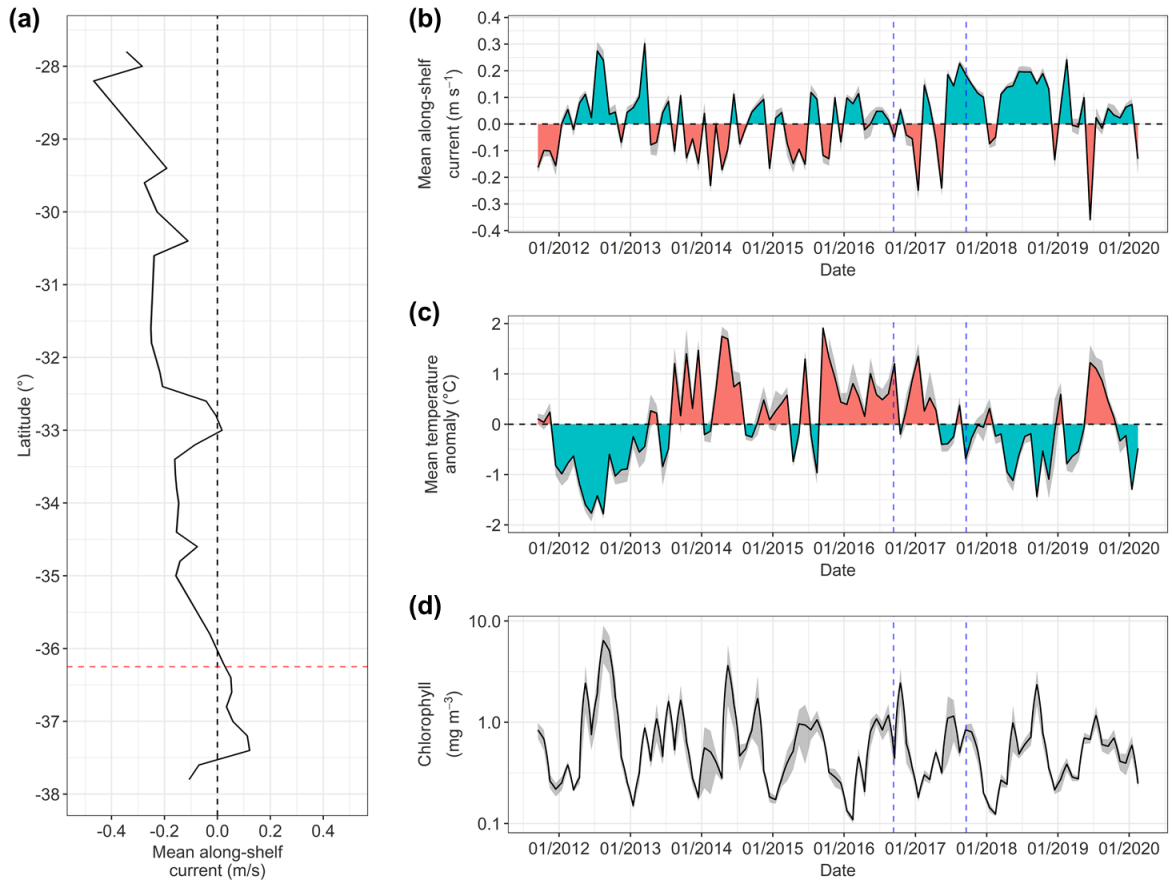

Figure 3. Mean along shelf current for southeast Australia along the 200 m isobath (a) with red dashed line indicating the latitude of Montague Island. For this location, monthly aggregated time-series for current direction (b) temperature anomaly (c) and Chl-*a* concentration (d) along the shelf edge are displayed. For (b), blue shading indicates net northward flow and red shading for net southward flow. For (c), blue shading indicates negative temperature anomaly and red shading for positive temperature anomaly. Grey shading indicates the standard error of the mean for all panels. Black dashed lines indicate the point of zero flow (a, b) or temperature anomaly (c). Blue dashed lines (b, c, d) correspond with the dates of the two surveys.

Long-term sea surface temperature anomaly (Fig. 3c) indicated a moderate negative correlation with along-shelf current velocity (coefficient = -3.06, n = 102, R^2 = 0.21, p < 0.001), indicating that variability in temperature was affected by the alternating influence of EAC and Tasman Sea water. Long-term temperature data indicated that the 2016 survey was conducted during a period of positive temperature anomaly (1.1 ± 0.2 °C), while the 2017 survey was conducted at a time of negative temperature anomaly (-0.6 ± 0.1 °C).

Temperature-salinity plots produced from underway data provide further evidence for a separation in water mass signatures between the two surveys (Fig. 4).

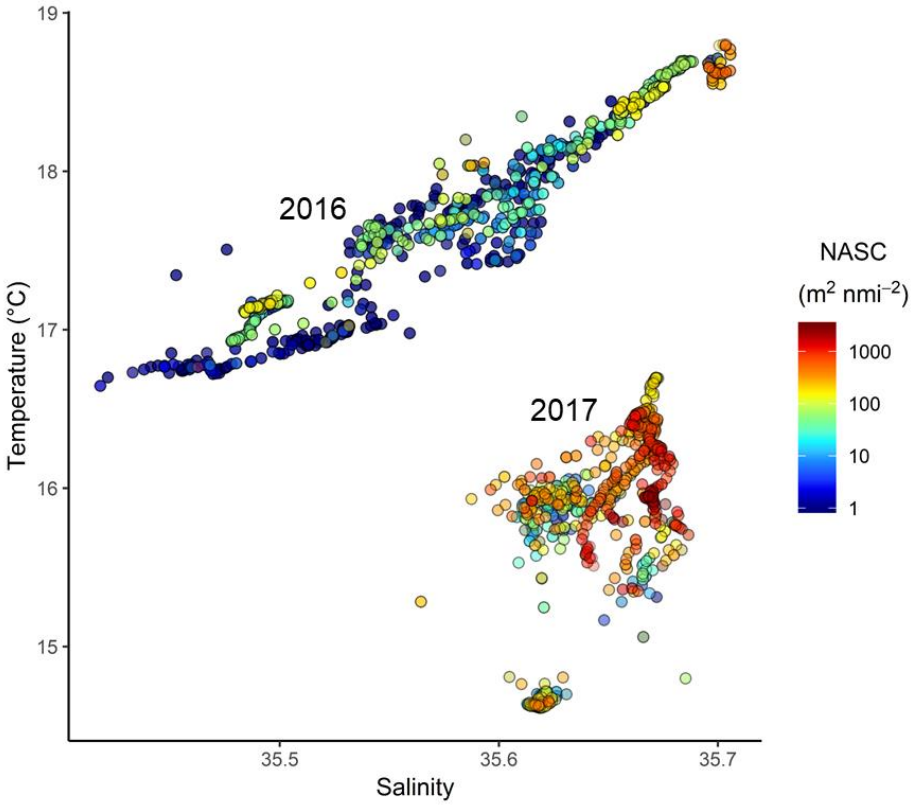

Fig. 4. Temperature-salinity plots generated from the ship's underway data displaying NASC values from fish as point colour on a logarithmic scale for each of the two surveys.

This long-term satellite data indicated that the $\log_{10}$ of Chl-*a* concentration (Fig. 3d) was negatively correlated with water temperature (coefficient = -0.11, n = 102, $R^2 = 0.43$, $p < 0.001$), with the annual peak in Chl-*a* concentration generally occurring in early spring, when water temperatures were at their annual minimum. The annual cycle of Chl-*a* concentration suggested that both surveys were conducted during this spring bloom, with a mean concentration (± SE) of 0.44 ± 0.09 mg m^{-3} in September 2016 and 0.84 ± 0.11 mg m^{-3} in September 2017.

The distribution of fishing operations in the region for the months of August to October (n = 67) was concentrated around 17.7 °C for trawls that caught *T. declivis* and 17.6 °C for trawls that caught *S. australasicus* (Supplement Fig. 5) while the background mean temperature was

17.2 °C. For both species, 90% of catch was caught in water above 17.1 °C. The mean temperature anomaly from the background (weighted by CPUE) was +0.24 °C for *T. declivis* ($p < 0.001$) and +0.31 °C for *S. australasicus* ($p < 0.001$). This temperature difference, although small, was consistently positive for both targeted species.

3.2. Comparing fish distribution between surveys

In both years, NASC was greatest in water with relatively high salinity and temperature (Fig. 4). There was greater overall NASC (mean ± SE) recorded in the 2017 survey (360 ± 12 m^2 nmi^{-2}) than in the 2016 survey (39 ± 1 m^2 nmi^{-2}, $f_{1,3898} = 1286$, $p < 0.001$). In 2016 mean NASC was greatest to the southeast of Montague Island (Fig. 5a) in the region along the shelf break (polygon S2.3: 136 ± 10.7 m^2 nmi^{-2}; $f_{11,2483} = 81$, $p < 0.001$) while the lowest NASC was recorded south of the island along the coast (polygon S1.1: 0.1 ± 0.06 m^2 nmi^{-2}). There was no significant difference among the four polygons adjacent to the coast ($f_{3,658} = 1.4$, $p = 0.246$). Comparing complete longitudinal bands (each band of four latitudinally-divided polygons), there was a statistically-significant gradient of increasing NASC from the coast to the shelf break (coast: 3.4 ± 1.1, mid: 38.6 ± 1.4, shelf: 70.9 ± 4.2 m^2 nmi^{-2}; $f_{2,2492} = 162$, $p < 0.001$). In 2017 the greatest mean NASC was also recorded to the southeast of the island (Fig. 5b, polygon S2.2: 894 ± 43 m^2 nmi^{-2}; $f_{11,1393} = 89$, $p < 0.001$). Similar to the 2016 survey, the lowest values were recorded along the coast (polygon S1.1: 89 ± 12 m^2 nmi^{-2}) and there was a similar coast to shelf gradient (coast: 112.7 ± 8.6, mid: 472.5 ± 23.3, shelf: 522.5 ± 17.9 m^2 nmi^{-2}; $f_{2,1402} = 148$, $p < 0.001$).

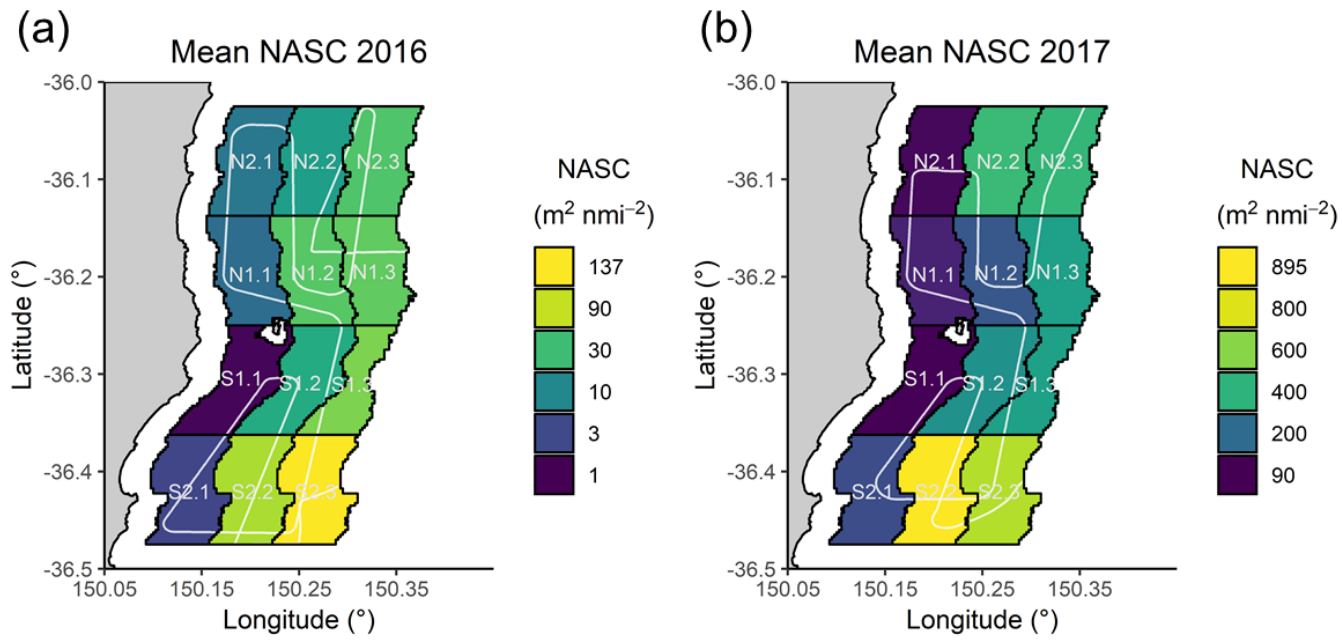

Fig. 5. Mean NASC values for each of twelve polygons of equal interval latitude and longitudinal spacing from the coast bounded in the central latitude by Montague Island for the 2016 survey (a) and the 2017 survey (b). Polygons are labelled so they can be referenced in text. Note both panels use a different colour scale and polygons are approximately 70 km^2.

Using nearest neighbour matching (Supplement Fig. 6) we were able to geographically pair 79% of NASC measurements from 2017 with measurements from 2016 (n = 1107). The $\log_{10}$(NASC) of both surveys were significantly and positively correlated ($r = 0.40$, $t_{1105} = 14$, $p < 0.001$). This indicates a moderate degree of correlation among spatially co-located measurements between the two surveys, despite the different oceanographic conditions and overall greater NASC in 2017.

3.3. Bathymetry as a driver of fish and zooplankton vertical distribution

The mean bottom depths of each of the three transects north of Montague Island were 62, 100 and 118 m. Zooplankton biomass (± SE) at the surface was 4143 ± 344 mg m^{-3} for the transect nearest to the coast and 461 ± 90 mg m^{-3} for the transect nearest to the shelf break (Fig. 6a). There was a 3.8-fold increase in biomass between the surface and 50 m depth for the shallowest transect in comparison to a 13.5-fold increase in biomass across the same depth range for the deepest transect. The decline in zooplankton biomass with depth was less

steep along the coast than it was offshore (GLM, 62 m isobath: coef. = 1.034; 118 m isobath: coef. = 1.059; $p < 0.0001$).

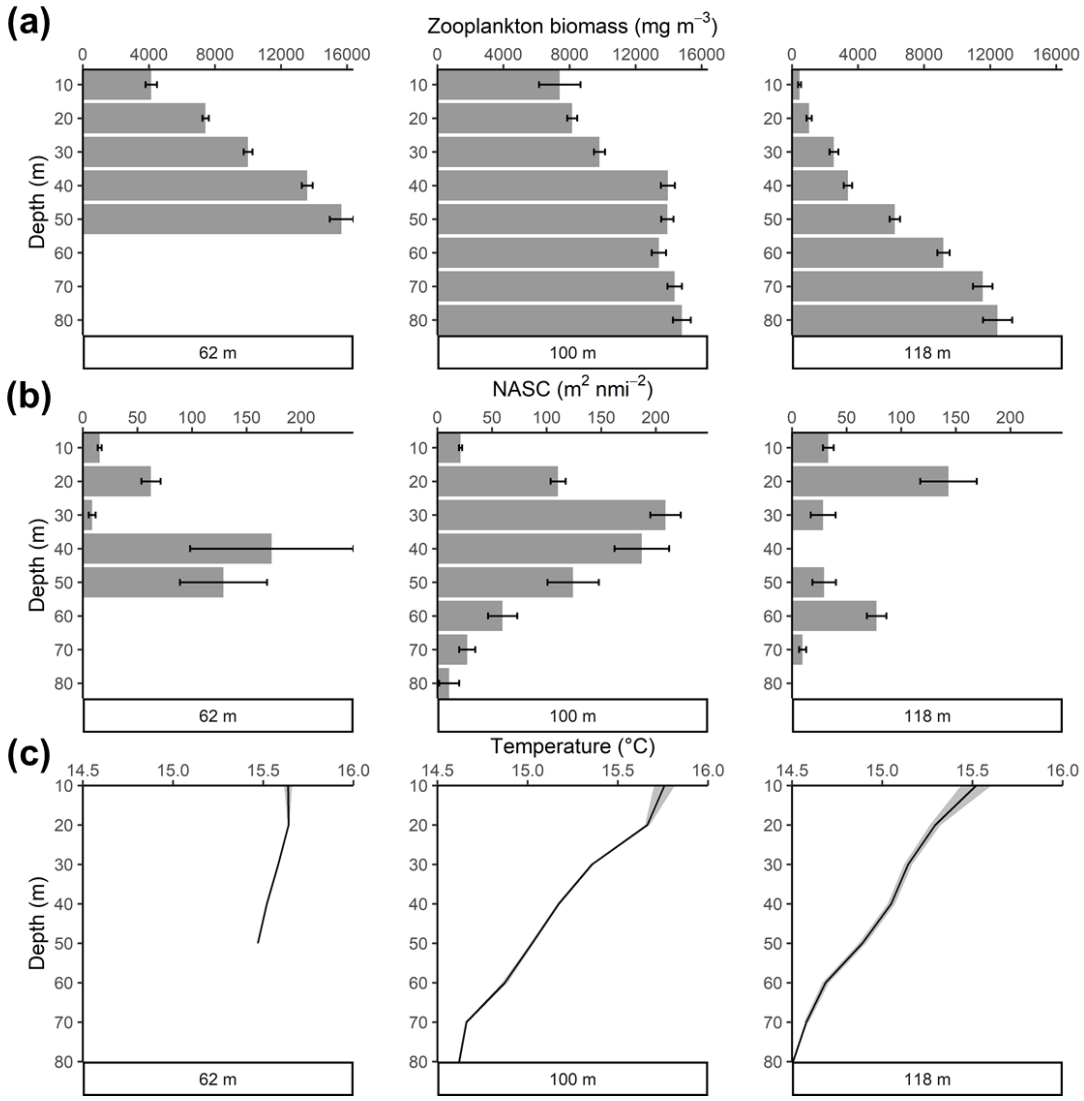

Fig. 6. Vertical distribution of mean zooplankton biomass (a), mean fish NASC (b) and mean temperature (c) for three along-shelf transects with mean bathymetry (62, 100 and 118 m bottom depth) from the 2017 survey. Error bars (a,b) and ribbon width (c) represent standard error.

In surface waters (<30 m from the surface), NASC from fish was greater offshore than in coastal waters. The peak in NASC, with respect to water depth, became increasingly shallow with increasing distance from the coast (Fig. 6b). The greatest NASC from fish for the most coastal transect (± SE) occurred at 40 m depth (173 ± 75 m^2 nmi^2), while for the furthest offshore transect the peak in NASC occurred at 20 m depth (143 ± 26 m^2 nmi^2). Although

surface temperatures (as measured by the towed-body) were similar across all three bottom depths (15.6, 15.8, 15.5°C from shallow to deep, respectively), there was a much faster decline in temperature with depth offshore, ranging between 14.9 to 15.5°C, while temperature only ranged between 15.5 to 15.6°C for the most coastal transect.

3.4. Modelling and predicting fish and zooplankton surface distribution

The initial NASC linear models with bathymetry as the only predictor met all assumptions of normality (2016: n = 2841, 2017: n = 1572). Coefficient and intercept estimates (± SE) indicated an elevated and more consistent overall NASC in 2017 (coef. = 0.03 ± 0.001, int. = 2.67 ± 0.12) compared with 2016 (coef. = 0.06 ± 0.003, int. = -2.93 ± 0.27) across the range of bathymetry surveyed.

Following this, we generated NASC models which included temperature and Chl-*a* as additional covariates (Table 2). In both cases bathymetry and temperature were selected to explain further variation in the forward-stepwise variable selection process, resulting in the two final models with identical structure described (Fig. 7a,b).

Table 2. The three sets of models selected via the forward-stepwise AIC-based selection process for NASC in 2016 (NASC.2016), NASC in 2017 (NASC.2017) and zooplankton biomass in 2017. In this case, ΔAIC represents the difference in AIC between the most parsimonious model and the model specified. Columns named after variables correspond to coefficient and intercept estimates and p values are indicated for each predictor variable where appropriate.

Model formula	ΔAIC	Int	Int p	Bath	Bath p	Temp	Temp p	log_{10}(chl)	log_{10}(chl) p	log_{10}(zoo)	log_{10}(zoo) p
NASC.2016 ~ bathymetry + temperature	0.00	-12.81	<0.001	0.05	<0.001	0.56	<0.001	-	-	-	-
NASC.2016 ~ bathymetry	104.93	-2.93	<0.001	0.06	<0.001	-	-	-	-	-	-
NASC.2016 ~ 1	1054.36	3.77	<0.001	-	-	-	-	-	-	-	-
NASC.2017 ~ bathymetry + temperature + log10(zooplankton)	0.00	-6.94	<0.001	0.02	<0.001	0.72	<0.001	-	-	-0.24	0.079
NASC.2017 ~ bathymetry + temperature	0.55	-2.28	0.011	0.03	<0.001	0.34	<0.001	-	-	-	-
NASC.2017 ~ bathymetry	39.61	2.67	<0.001	0.03	<0.001	-	-	-	-	-	-

NASC.2017 ~ 1	363.57	5.89	<0.001	-	-	-	-	-	-	-	-
Zooplankton Biomass ~ log_{10}(chlorophyll) + bathymetry + temperature	0.00	3.14	0.008	-0.01	<0.001	0.42	<0.001	2.20	<0.001	-	-
Zooplankton Biomass ~ log_{10}(chlorophyll) + bathymetry	33.42	9.04	<0.001	-0.01	0.001	-	-	3.01	<0.001	-	-
Zooplankton Biomass ~ log_{10}(chlorophyll)	46.90	8.56	<0.001	-	-	-	-	3.36	<0.001	-	-
Zooplankton Biomass ~ 1	144.36	8.64	<0.001	-	-	-	-	-	-	-	-

We subsequently included zooplankton biomass as an additional predictor within the 2017 model (the only year for which we have zooplankton biomass) but this did not explain any additional variability in NASC (Table 2, Fig. 7c), as the inclusion of this additional predictor only improved AIC by 0.55. The zooplankton biomass model retained all three of its initial predictors in the variable selection process and Chl-*a* explained the greatest amount of variation in the response, followed by bathymetry and temperature respectively (Fig. 7d).

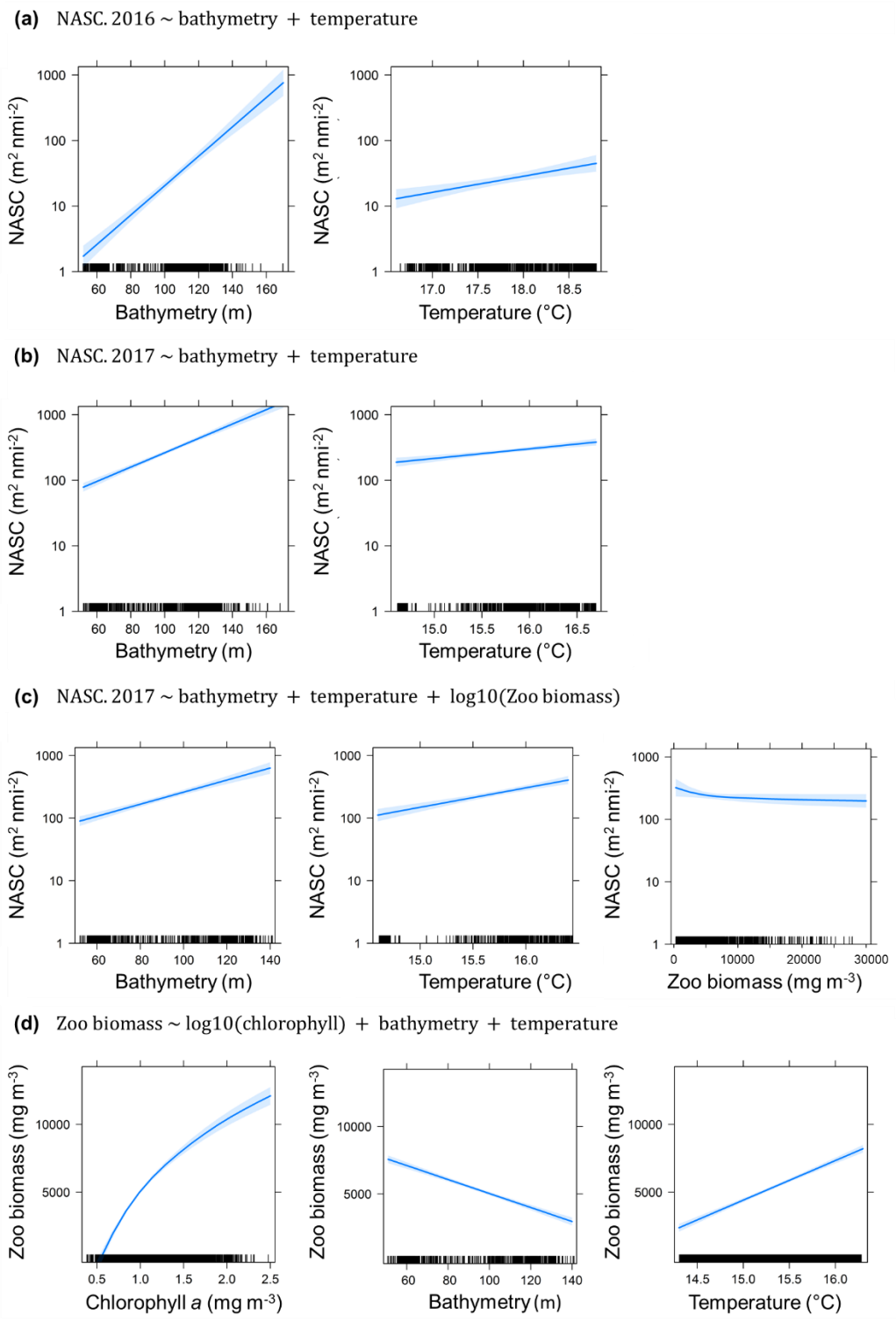

Fig. 7. Model structure and predictor responses for the most parsimonious models for fish NASC in 2016 (a) and 2017 (b) and with the additional predictor for zooplankton biomass (c) which was not selected in the most parsimonious model, and the model for zooplankton biomass from the 2017 survey (d).

Examination of the autocorrelation function indicated that some degree of serial

autocorrelation was present in all models, at scales ranging from ~ 2 km for the zooplankton

biomass models to ~ 4 km for the NASC models from both years. Our adjusted inference (Supplement Table 2) took this into account by using HAC estimates to adjust the test statistic accordingly for all model predictors. All predictors which demonstrated statistical significance ($p < 0.05$) in the original inference remained significant after HAC estimates were included, except for the effect of Chl-*a* on zooplankton biomass.

3.5. Comparing fish and zooplankton predicted surface distribution

Spatial model predictions of NASC were generated for each of the two fish models (Fig. 7a,b) using bathymetry and sea surface temperature as predictors (Fig. 8a,b). There were some differences in the distribution of NASC from fish across the two predictions, even though a static variable (bathymetry) predicted most of the variability in both models. Overall, predicted NASC (± SE) in 2017 (430.7 ± 11.0 m^2 nmi^{-2}) was higher than 2016 (100.5 ± 5.8 m^2 nmi^{-2}). In 2016 there was a much steeper decrease in NASC between the shelf break and the coast. Standardised proportional differences in the distribution of NASC between years (Fig. 8d) indicated that overall variation was low (mean = 15%), while 80% of the study area showed less than 25% variation. The greatest variability in NASC between surveys occurred along the edge of the continental shelf, driven by variation in water temperature.

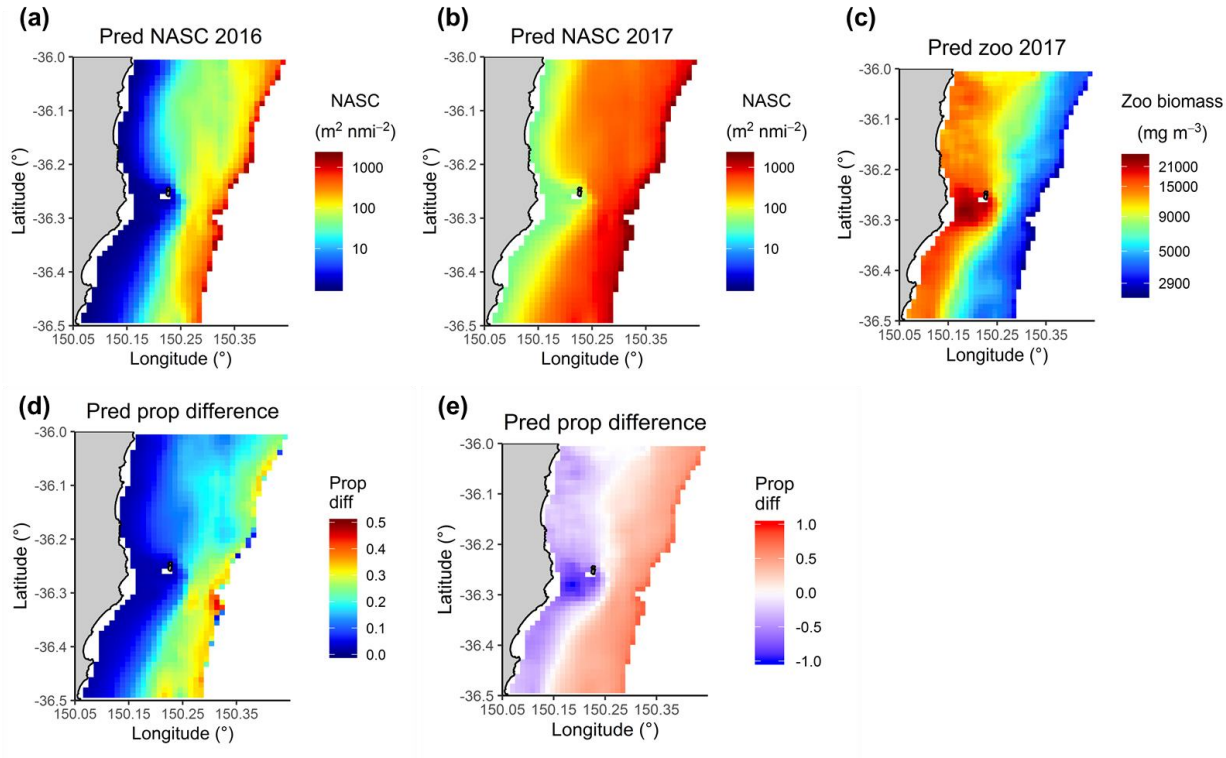

Fig. 8. Model prediction results for pelagic forage fish in 2016 (a) and 2017 (b), and for zooplankton biomass (c), generated using satellite data and bathymetry maps. Absolute proportional differences in the standardised distribution of fish between the 2016 (a) and 2017 (b) surveys is represented by (d). Proportional differences in the simultaneous distribution of zooplankton (c) and fish at the time of the 2017 survey (b) is represented by (e), with negative values indicating greater proportional density of zooplankton and positive values indicating greater proportional presence of NASC from fish (relative to the entire study area).

The additional prediction (Fig. 8c) generated from the zooplankton biomass model for 2017 (Fig. 7d), using MODIS satellite Chl-*a*, sea surface temperature and bathymetry as predictors displayed an almost opposite distribution to NASC in the same survey (Fig. 8b), as evidenced by the plot of the difference in standardised NASC and zooplankton biomass (Fig. 8e). The proportional difference plot indicated greatest zooplankton biomass along the coast and greatest NASC from fish along the shelf break.

4. DISCUSSION

Our research reveals new insights into the spatial dynamics of forage fish and their prey in temperate coastal waters that form a key foraging area for iconic marine fauna (Carroll et al. 2017). We found moderate inter-annual consistency in the spatial distribution of forage fish (r

= 0.40), despite a reversal in current direction which reduced the influence of the EAC in favour of colder, more productive Tasman Sea water in 2017. Such reversals in current direction are common for this coastal region (Fig. 3b), driving alternate influences of cold and warm water masses.

We found that springtime distribution of water temperature played a more important role than zooplankton density, both vertically and horizontally, in structuring the daytime distribution of forage fish (Fig. 1). In this case, it was apparent that their balance of needs was skewed towards prioritising thermal requirements over locating the highest densities of prey. Furthermore, we found that the shelf break is an important habitat for schools of forage fish in spring. Despite the paucity of zooplankton available in surface waters along the shelf break, there may be adequate zooplankton available for forage fish at dawn or dusk as these trophic groups converge during diel vertical migration.

4.1. Bathymetry as a driver of fish distribution

While other studies have found evidence for consistent seasonal distribution of pelagic forage fish at large spatial scales (100s of kms; Maravelias 1999, Grémillet et al. 2008), we assumed at the scale of our study (10s of kms) that the distribution of forage fish in surface waters would be highly variable. However, we found evidence to suggest a degree of relative similarity in fish distribution from the coast to the shelf break between annual surveys, despite variations in temperature and the large differences in current velocity and direction as well as Chl-*a*. A strong driver of this consistent distribution is a positive correlation with bathymetry, as the greatest densities of forage fish in surface waters of the continental shelf were located along the shelf break and associated with warmer offshore water in both 2016 and 2017. Differences in the distribution of water masses between surveys are a potential driver for the smaller interannual variation we observed in fish distribution between surveys,

and this was reflected by our model predictions that showed only 15% mean variation between surveys.

Along the shelf break, high densities of fish were observed near the surface in both surveys and density declined with depth. Surface waters along the coast showed an opposite pattern, with low fish density at the surface and higher density near the seafloor. The horizontal gradient in fish density was steepest in the 2016 survey. Other studies in the North Sea have documented similar findings, with the greatest densities of Atlantic herring (*Clupea harengus*) associated with deeper areas of the continental shelf near the shelf break, and with specific substrate types (Maravelias 1999). It seems likely that this spatial pattern is related to other biological processes not measured in this study that may be associated indirectly with depth. For example, blue mackerel (*Scomber australasicus*), which we know to be prevalent in the region (Marton and Steven 2019), congregates at lower latitudes along the shelf break to spawn (Neira and Keane 2008). However, this strong association with the shelf break is not just limited to times when fish are spawning, it may also be preferred in foraging periods (Maravelias 1999). The positive relationship with bathymetry and the distribution of pelagic forage fish could also be influenced by an inshore-offshore gradient in perceived predation risk.

Little penguins nesting on Montague Island tend to feed in the top 20 m of the water column on the inshore side of the island during daytime foraging trips (Carroll et al. 2016, Carroll et al. 2017). There is also evidence that fur seals forage in water depths of 60-80 m (Arnould and Kirkwood 2007). Similar to zooplankton, pelagic fish are topographically constrained within shallow coastal environments (Aarflot et al. 2019), which puts them in closer proximity to both benthic (Woodland and Secor 2013) and surface predators such as seabirds (Maxwell and Morgan 2013). Thus, shallower regions of the shelf in the vicinity of the island present a high predation risk for forage fish. Other studies have demonstrated that forage fish

will avoid areas with relatively high predation risk, even if this avoidance restricts them to lower-density food resources (Werner et al. 1983, Holbrook and Schmitt 1988, Logerwell and Hargreaves 1996). Thus, in our study region forage fish may be restricting their distribution to be further offshore, at least during the day when they are most susceptible to these visual predators. Penguins may similarly be feeding on the inshore side of the island on the small, patchy, and therefore more vulnerable, schools which occur away from their main distribution along the shelf break.

4.2. Temperature as a driver of fish distribution

Temperature increased from inshore to offshore in both surveys, however there was enough latitudinal variation in the dynamic distribution of warm water masses to separate the effects of bathymetry and temperature. Thus, the inter-survey variability in fish distribution in the outer shelf region is partially attributed to the redistribution of warm water masses. It is likely that this positive relationship with temperature is unimodal over a greater range of temperatures, given that our surveys were conducted in early spring (Castillo et al. 1996, Carroll et al. 2016). Zooplanktivorous fish dominate the biomass observed around rocky reefs in this region, however their biomass generally peaks here in early autumn when water temperatures are several degrees warmer (> 20°C) (Holland et al. 2020).

The primary catch of the local fishery is dominated by *T. novaezelandiae, T. declivis* and *S. australasicus* (Marton and Steven 2019). To determine the optimum temperature for each species, we calculated the average of the 10^{th} and 90^{th} preferable temperature percentiles from AquaMaps (Kaschner et al. 2008) in a method adapted from Serpetti et al. (2017). Calculated optimum temperatures were: 18.7°C for *T. novaezelandiae,* 17.2°C for *T. declivis* and 20.7°C for *S. australasicus* (Kaschner et al. 2008, Serpetti et al. 2017). The range of temperatures across our study area during the 2016 survey were 16.7 to 18.8°C while during the 2017 survey was 14.6 to 16.7°C, which were well-below the optimum temperatures calculated for

these three species. Only in 2016 were temperatures recorded which exceed the optimum temperatures for *T. novaezelandiae* and *T. declivis*, and these temperatures were only recorded along parts of the shelf break.

The combined fishery for *T. novaezelandiae* and *S. australasicus* in the region is highly linked to temperature, as these fish largely disappear in winter when water temperatures drop below 13°C (Stewart and Ferrell 2001). These two species do not return in large numbers until water temperatures reach 17°C in summer, between November and January (Stewart and Ferrell 2001). As spring temperatures during our surveys were likely below the thermal optimum for most forage fish species that inhabit the area, it is likely that fish were actively seeking out warmer water through behavioural thermoregulation (Magnuson et al. 1979).

Nevertheless, across the entire study area, there was higher fish density in the 2017 survey (9-fold increase in mean NASC), even though mean water temperature was 2°C cooler than 2016. In this case, the higher chlorophyll in the colder Tasman Sea water may have had some influence on the increased density of fish in the area. It is possible that the positive effect of temperature on forage fish may be related to relative temperature (not absolute) and it could also be related to zooplankton biomass or their perceived risk of predation.

4.3. Spatial mismatch of predators and prey

There was a mismatch in the distribution of pelagic forage fish and zooplankton, with the greatest densities of fish found offshore, while the greatest densities of zooplankton were found close to the coast (Fig. 8e). The model variable selection process indicated that Chl-*a* was the most influential variable that correlated with the density of zooplankton. Several studies have concluded that zooplankton density is driven by bottom-up processes, so their distribution may be driven by phytoplankton abundance (Canfield and Watkins 1984, Strömberg et al. 2009). However, the results of inference and our examination of zooplankton

distribution with depth over three levels of bathymetry suggests that topographic constraints may be a more important driver in our study area (Genin 2004, Aarflot et al. 2019).

We observed a much steeper decline in zooplankton density with depth from the surface along the shelf break than near the coast (Fig. 6a). This pattern is typical of a topographic blockage, when zooplankton are advected onto shallow shelf waters at night and their pre-dawn descent is blocked by shallow bathymetry (Genin 2004). Despite this gradient in zooplankton, we found the peak in fish density with depth shallowed with increasing distance offshore or bottom depth (Fig. 6b). This may have played a role in driving the observed pattern of greater fish density in surface waters along the shelf break and may be related to temperature.

There are large overall differences in the way water temperature and zooplankton are spatially distributed, which could at least partially explain this mismatch. Fish migrate through a dynamic seascape to optimise their physiological performance. A major assumption of ideal free distribution (IFD) theory is that foragers have perfect knowledge of the quality and distribution of resource patches within their environment (Tregenza 1995, Matsumura et al. 2010). Variation in temperature is more predictable than zooplankton patches and generally occurs gradually and over a coarser spatial scale than zooplankton distribution. If temperature is an ecological resource (Magnuson et al. 1979), it may be easier for fish to navigate to optimal thermal conditions than it is for them to locate optimal foraging conditions.

Sato et al. (2018) found that in the Northern California Current System forage fish distribution shifted offshore to remain in warmer water as summer upwelling intensified and the upwelling front moved cold water further offshore. As the EAC is strengthening with climate change (Ridgway 2007), topographically induced upwelling intensity in our study

area is also expected to increase in the coming decades. This could cause upwelling fronts to expand, shifting cold water further offshore of the shelf break and likely shifting forage fish distribution along with them. This may impact the colonies of little penguins and fur seals which nest and pup on Montague Island and are limited in the distance they can travel on daily foraging trips (Carroll et al. 2017).

Our analysis of two surveys showed the distribution of pelagic forage fish across our study region showed consistent relationships with bathymetry and temperature. Overall, our findings suggest that in periods when temperatures are sub-optimal and the distributions of prey and warm water do not align, forage fish may prioritise thermoregulation over optimised foraging. In the coldest months when temperatures are well below optimal it is possible that even minor increases in body temperature may provide substantial benefits for improved somatic growth (Neuheimer and Taggart 2007, Neuheimer et al. 2011). However, in seasons when temperatures are closer to the thermal optima for specific taxa (Holland et al. 2020), this balance may shift to prioritise improved foraging.

To resolve these relationships, we suggest day and night surveys in other seasons to explore the horizontal and vertical relationships among zooplankton, forage fish and water temperature. The oceanographic bidirectionality in current flow at the poleward end of a western boundary current is intriguing, especially around an important foraging ground for seals, whales and penguins. With water temperatures along western boundary currents rising at rates two to three times the global average (Wu et al. 2012), it is becoming increasingly important that we understand what motivates the behaviour of these highly mobile and temperature-dependent species, so that we can forecast their future distribution.

ACKNOWLEDGEMENTS

Many thanks to the scientific staff and crew of the *RV Investigator* who safely and successfully navigated us around Montague Island, to Sven Gastauer (Scripps Institute of Oceanography) for his catch data and expertise in operating the acoustic instruments in 2017, and to Leonardo Laiolo (CSIRO) and David Suggett (University of Technology Sydney) for providing their Chl-*a* measurements, and to Sally Weekes and Selvy Coundjidapadam from the Australian Fisheries Management Authority (AFMA) for providing the catch data. This work was funded by an Australian Government Research Training Program Scholarship. IMS and JDE were supported by the ARC (LP120100592, DP150102656) and MMH was supported by a Research Training Program PhD scholarship. Data was sourced from the Integrated Marine Observing System (IMOS) - IMOS is a national collaborative research infrastructure, supported by the Australian Government.

LITERATURE CITED

Aarflot, J. M., D. L. Aksnes, A. F. Opdal, H. R. Skjoldal, and Ø. Fiksen. 2019. Caught in broad daylight: Topographic constraints of zooplankton depth distributions. Limnology and Oceanography **64**:849-859.

Arnould, J. P., and R. Kirkwood. 2007. Habitat selection by female Australian fur seals (*Arctocephalus pusillus doriferus*). Aquatic Conservation: Marine and Freshwater Ecosystems **17**:S53-S67.

Arya, S., D. Mount, S. Kemp, and G. Jefferis. 2017. RANN: Fast nearest neighbour search (wraps ANN library) Using L2 metric, R package version 2.5. 1.

Ayón, P., G. Swartzman, A. Bertrand, M. Gutiérrez, and S. Bertrand. 2008. Zooplankton and forage fish species off Peru: large-scale bottom-up forcing and local-scale depletion. Progress in Oceanography **79**:208-214.

Bakun, A. 2006. Wasp-waist populations and marine ecosystem dynamics: navigating the "predator pit" topographies. Progress in oceanography **68**:271-288.

Bennett, S., T. Wernberg, S. D. Connell, A. J. Hobday, C. R. Johnson, and E. S. Poloczanska. 2016. The 'Great Southern Reef': social, ecological and economic value of Australia's neglected kelp forests. Marine and Freshwater Research **67**:47-56.

Benoit-Bird, K. J., and M. A. McManus. 2012. Bottom-up regulation of a pelagic community through spatial aggregations. Biology Letters **8**:813-816.

Canfield, D. E. J., and C. E. Watkins. 1984. Relationships between zooplankton abundance and chlorophyll a concentrations in Florida lakes. Journal of Freshwater Ecology **2**:335-344.

Carroll, G., M. Cox, R. Harcourt, B. J. Pitcher, D. Slip, and I. Jonsen. 2017. Hierarchical influences of prey distribution on patterns of prey capture by a marine predator. Functional Ecology **31**:1750-1760.

Carroll, G., J. D. Everett, R. Harcourt, D. Slip, and I. Jonsen. 2016. High sea surface temperatures driven by a strengthening current reduce foraging success by penguins. Scientific reports **6**:22236.

Castillo, J., M. Barbieri, and A. Gonzalez. 1996. Relationships between sea surface temperature, salinity, and pelagic fish distribution off northern Chile. ICES Journal of Marine Science **53**:139-146.

Cetina- Heredia, P., M. Roughan, E. Van Sebille, and M. Coleman. 2014. Long- term trends in the East Australian Current separation latitude and eddy driven transport. Journal of Geophysical Research: Oceans **119**:4351-4366.

De Robertis, A., and I. Higginbottom. 2007. A post-processing technique to estimate the signal-to-noise ratio and remove echosounder background noise. ICES Journal of Marine Science **64**:1282-1291.

Everett, J., M. Baird, P. Oke, and I. Suthers. 2012. An avenue of eddies: Quantifying the biophysical properties of mesoscale eddies in the Tasman Sea. Geophysical Research Letters **39**.

Genin, A. 2004. Bio-physical coupling in the formation of zooplankton and fish aggregations over abrupt topographies. Journal of Marine Systems **50**:3-20.

Grémillet, D., S. Lewis, L. Drapeau, C. D. van Der Lingen, J. A. Huggett, J. C. Coetzee, H. M. Verheye, F. Daunt, S. Wanless, and P. G. Ryan. 2008. Spatial match–mismatch in the Benguela upwelling zone: should we expect chlorophyll and sea- surface temperature to predict marine predator distributions? Journal of Applied Ecology **45**:610-621.

Holbrook, S. J., and R. J. Schmitt. 1988. The combined effects of predation risk and food reward on patch selection. Ecology **69**:125-134.

Holland, M. M., J. A. Smith, J. D. Everett, A. Vergés, and I. M. Suthers. 2020. Latitudinal patterns in trophic structure of temperate reef-associated fishes and predicted consequences of climate change. Fish and Fisheries **In press**.

Holmes, T. H., S. K. Wilson, M. J. Travers, T. J. Langlois, R. D. Evans, G. I. Moore, R. A. Douglas, G. Shedrawi, E. S. Harvey, and K. Hickey. 2013. A comparison of visual- and stereo- video based fish community assessment methods in tropical and temperate marine waters of Western Australia. Limnology and Oceanography: Methods **11**:337-350.

Hwang, K., E.-A. Yoon, K. Lee, H. Lee, and D.-J. Hwang. 2015. Multifrequency acoustic scattering characteristics of jack mackerel by KRM model. Journal of the Korean Society of Fisheries and Ocean Technology **51**:424-431.

Integrated Marine Observing System. 2018. IMOS - SRS - MODIS - 01 day - Ocean Colour - SST.

Johnson, N. L., S. Kotz, and N. Balakrishnan. 1970. Continuous univariate distributions. Houghton Mifflin Boston.

Kaschner, K., J. Ready, E. Agbayani, J. Rius, K. Kesner-Reyes, P. Eastwood, A. South, S. Kullander, T. Rees, and C. Close. 2008. AquaMaps: Predicted range maps for aquatic species. World wide web electronic publication, wwwaquamapsorg, Version **10**:2008.

Korneliussen, R. J., and E. Ona. 2002. An operational system for processing and visualizing multi-frequency acoustic data. ICES Journal of Marine Science **59**:293-313.

Logerwell, E. A., and N. B. Hargreaves. 1996. The distribution of sea birds relative to their fish prey off Vancouver Island: opposing results at large and small spatial scales. Fisheries Oceanography **5**:163-175.

Longo, G. O., M. E. Hay, C. E. Ferreira, and S. R. Floeter. 2019. Trophic interactions across 61 degrees of latitude in the Western Atlantic. Global ecology and biogeography **28**:107-117.

Lucas, A. J., C. L. Dupont, V. Tai, J. L. Largier, B. Palenik, and P. J. Franks. 2011. The green ribbon: Multiscale physical control of phytoplankton productivity and community structure over a narrow continental shelf. Limnology and Oceanography **56**:611-626.

MacLennan, D. N., P. G. Fernandes, and J. Dalen. 2002. A consistent approach to definitions and symbols in fisheries acoustics. ICES Journal of Marine Science **59**:365-369.

Magnuson, J. J., L. B. Crowder, and P. A. Medvick. 1979. Temperature as an ecological resource. American Zoologist **19**:331-343.

Maravelias, C. D. 1999. Habitat selection and clustering of a pelagic fish: effects of topography and bathymetry on species dynamics. Canadian Journal of Fisheries and Aquatic Sciences **56**:437-450.

Marton, N., and A. Steven. 2019. Chapter 7: Small Pelagic Fishery. Australian Bureau of Agricultural and Resource Economics and Sciences, Canberra.

Matsumura, S., R. Arlinghaus, and U. Dieckmann. 2010. Foraging on spatially distributed resources with sub- optimal movement, imperfect information, and travelling costs: departures from the ideal free distribution. Oikos **119**:1469-1483.

Maxwell, S. M., and L. E. Morgan. 2013. Foraging of seabirds on pelagic fishes: implications for management of pelagic marine protected areas. Marine Ecology Progress Series **481**:289-303.

McInnes, A. M., P. G. Ryan, M. Lacerda, J. Deshayes, W. S. Goschen, and L. Pichegru. 2017. Small pelagic fish responses to fine-scale oceanographic conditions: implications for the endangered African penguin. Marine Ecology Progress Series **569**:187-203.

McKelvey, D. R., and C. D. Wilson. 2006. Discriminant classification of fish and zooplankton backscattering at 38 and 120 kHz. Transactions of the American Fisheries Society **135**:488-499.

Miyanohana, Y., K. Ishii, and M. Furusawa. 1990. Measurements and analyses of dorsal-aspect target strength of six species of fish at four frequencies. Rapports et Proces-Verbaux des Réunions du Conseil International pour l'Exploration de la Mer **189**:317-324.

Neira, F. J., and J. P. Keane. 2008. Ichthyoplankton- based spawning dynamics of blue mackerel (*Scomber australasicus*) in south- eastern Australia: links to the East Australian Current. Fisheries Oceanography **17**:281-298.

Neuheimer, A., R. Thresher, J. Lyle, and J. Semmens. 2011. Tolerance limit for fish growth exceeded by warming waters. Nature Climate Change **1**:110.

Neuheimer, A. B., and C. T. Taggart. 2007. The growing degree-day and fish size-at-age: the overlooked metric. Canadian Journal of Fisheries and Aquatic Sciences **64**:375-385.

Pauly, D., R. Watson, and J. Alder. 2005. Global trends in world fisheries: impacts on marine ecosystems and food security. Philosophical Transactions of the Royal Society B: Biological Sciences **360**:5-12.

Pikitch, E., P. D. Boersma, I. Boyd, D. Conover, P. Cury, T. Essington, S. Heppell, E. Houde, M. Mangel, and D. Pauly. 2012. Little fish, big impact: managing a crucial link in ocean food webs. Lenfest Ocean Program, Washington, DC **108**.

Pikitch, E. K., K. J. Rountos, T. E. Essington, C. Santora, D. Pauly, R. Watson, U. R. Sumaila, P. D. Boersma, I. L. Boyd, and D. O. Conover. 2014. The global contribution of forage fish to marine fisheries and ecosystems. Fish and Fisheries **15**:43-64.

Pribyl, A. L., J. R. Hyde, L. Robertson, and R. Vetter. 2016. Defining an ideal temperature range for the northern subpopulation of Pacific sardine, *Sardinops sagax caeruleus*. Environmental biology of fishes **99**:275-291.

R Core Team. 2018. R: A language and environment for statistical computing.

Ridgway, K. 2007. Long- term trend and decadal variability of the southward penetration of the East Australian Current. Geophysical Research Letters **34**.

Ryan, T. E., R. A. Downie, R. J. Kloser, and G. Keith. 2015. Reducing bias due to noise and attenuation in open-ocean echo integration data. ICES Journal of Marine Science **72**:2482-2493.

Sala, E., E. Ballesteros, P. Dendrinos, A. Di Franco, F. Ferretti, D. Foley, S. Fraschetti, A. Friedlander, J. Garrabou, H. Guclusoy, P. Guidetti, B. S. Halpern, B. Hereu, A. A. Karamanlidis, Z. Kizilkaya, E. Macpherson, L. Mangialajo, S. Mariani, F. Micheli, A. Pais, K. Riser, A. A. Rosenberg, M. Sales, K. A. Selkoe, R. Starr, F. Tomas, and M. Zabala. 2012. The structure of Mediterranean rocky reef ecosystems across

environmental and human gradients, and conservation implications. PloS one **7**:e32742.

Sato, M., J. A. Barth, K. J. Benoit-Bird, S. D. Pierce, T. J. Cowles, R. D. Brodeur, and W. T. Peterson. 2018. Coastal upwelling fronts as a boundary for planktivorous fish distributions. Marine Ecology Progress Series **595**:171-186.

Schilling, H. 2014. Zooplankton biomass variability and the impact of fish foraging along an estuarine gradient. Honours thesis. The University of New South Wales.

Serpetti, N., A. R. Baudron, M. Burrows, B. L. Payne, P. Helaouet, P. G. Fernandes, and J. Heymans. 2017. Impact of ocean warming on sustainable fisheries management informs the Ecosystem Approach to Fisheries. Scientific reports **7**:13438.

Shaughnessy, P. D., S. V. Briggs, and R. Constable. 2001. Observations on seals at Montague Island, New South Wales. Australian Mammalogy **23**:1-7.

Stewart, J., and D. J. Ferrell. 2001. Age, growth, and commercial landings of yellowtail scad (*Trachurus novaezelandiae*) and blue mackerel (*Scomber australasicus*) off the coast of New South Wales, Australia. New Zealand Journal of Marine and Freshwater Research **35**:541-551.

Strömberg, K. P., T. J. Smyth, J. I. Allen, S. Pitois, and T. D. O'Brien. 2009. Estimation of global zooplankton biomass from satellite ocean colour. Journal of Marine Systems **78**:18-27.

Suthers, I. M., C. Taggart, D. Rissik, and M. Baird. 2006. Day and night ichthyoplankton assemblages and zooplankton biomass size spectrum in a deep ocean island wake. Marine Ecology Progress Series **322**:225-238.

Tregenza, T. 1995. Building on the ideal free distribution. Advances in ecological research **26**:253-307.

Ward , T. M., and G. L. Grammer. 2018. Commonwealth Small Pelagic Fishery: Fishery Assessment Report 2017. SARDI Research Report Series No. 982, South Australian Research and Development Institute (Aquatic Sciences), Adelaide.

Watson, R., A. Kitchingman, A. Gelchu, and D. Pauly. 2004. Mapping global fisheries: sharpening our focus. Fish and Fisheries **5**:168-177.

Werner, E. E., J. F. Gilliam, D. J. Hall, and G. G. Mittelbach. 1983. An experimental test of the effects of predation risk on habitat use in fish. Ecology **64**:1540-1548.

Whiteway, T. 2009. Australian bathymetry and topography grid. Geoscience Australia, Canberra.

Woodland, R. J., and D. H. Secor. 2013. Benthic- pelagic coupling in a temperate inner continental shelf fish assemblage. Limnology and Oceanography **58**:966-976.

Wu, L., W. Cai, L. Zhang, H. Nakamura, A. Timmermann, T. Joyce, M. J. McPhaden, M. Alexander, B. Qiu, and M. Visbeck. 2012. Enhanced warming over the global subtropical western boundary currents. Nature Climate Change **2**:161-166.

Zeileis, A. 2006. Object-oriented computation of sandwich estimators.

SUPPLEMENTARY INFORMATION

1.0. Methods

1.1. Classification methods

The 2016 and 2017 acoustic data were adjusted post collection, based on calibrations which were conducted on 17 August 2016 and 08 June 2018, respectively. Parameters such as transmission power and pulse duration were kept the same between voyages and gain adjustments drifted less than 0.3 dB from the 2016 calibration.

In both years, the EK60 transducers were synchronised and set to a pulse duration of 2.048 ms for the 18, 38 and 70 kHz and 1.024 ms for the 120, 200 and 333 kHz transducers with a ping rate of 1.11 Hz. Transmission power was set to 2000 W for the 18 and 38 kHz, 750 W for the 70 kHz, 250 W for the 120 kHz, 105 W for the 200 kHz and 40 W for the 333 kHz transducers.

In Echoview, seabed returns were manually verified and removed along with the first 5 m of water column below the transducer face to eliminate surface noise and ring down. Data was cleaned for removing background noise, impulse noise and transient noise prior to echo integration following the methods of De Robertis and Higginbottom (2007) and Ryan et al. (2015) through built-in functions in Echoview. Ping times and geometry were matched across all frequencies so that echoes from each frequency could be compared. Grid cells were sufficiently large to avoid issues of frequency-dependent sampling volume (Korneliussen and Ona 2002).

Grid cells were classified by employing a method similar to that applied by Korneliussen and Ona (2002), where multi-frequency data was used to derive relative frequency response signatures for samples they collected in situ. Since we only had fisheries catch records to inform which species may have been present, we used frequency response to guide our

classification. The frequency response of each grid cell was determined relative to the response for the 38 kHz band. Relative frequency response, *r(f)*, is defined as follows:

$$r(f) = \frac{S_v(f)}{S_{v38\ kHz}}$$

Where S_v is the volume backscattering coefficient of the grid cell, f is the acoustic frequency being queried and $S_{v38\ kHz}$ is the S_v of the 38 kHz band. Korneliussen and Ona (2002) made their comparisons using the following frequencies: 18, 38, 70, 120 and 200 kHz. As we did not have 120 kHz data for the 2017 survey (Table 1), we omitted this band from the analysis to ensure an identical classification method across the two surveys. Volume backscatter values were subject to set of logical criteria outlined in Korneliussen and Ona (2002) to classify cells which most likely contained fish schools. Cells were classified as containing fish if their relative backscatter decreased with increasing frequency or in other terms:

$$\frac{S_{v18\ kHz}}{S_{v\ 38\ kHz}} > 1 > \frac{S_{v70\ kHz}}{S_{v\ 38\ kHz}} > \frac{S_{v200\ kHz}}{S_{v\ 38\ kHz}}$$

For validation, we integrated sections of echograms which were visually identified to be likely fish schools and examined the resulting frequency response to inform our classification (Supplement Fig. 2). The trend of decreasing relative backscatter with increasing acoustic frequency is consistent with targets that are relatively strong scatterers, with gas-filled swim bladders (Miyanohana et al. 1990, Hwang et al. 2015). This frequency response is consistent with the acoustic scattering characteristics of Japanese horse mackerel (*Trachurus japonicus*), closely related to *T. declivis*, across a range of fork lengths from 134 to 190 mm (Hwang et al. 2015), and for *S. australasicus* between 216 and 360 mm (Miyanohana et al. 1990). Fisheries landing records from the 2016/17 season in our study region recorded the fork length range of these species to be 144 to 306 mm for *T. declivis* and 173 to 351 mm for *S. australasicus* (Ward and Grammer 2018).

1.2. Chlorophyll a methods

Chlorophyll *a* (Chl-*a*) was modelled from fluorescence by using laboratory-measured Chl-*a* determinations made with a Turner fluorometer (Turner Designs, San Jose, United States). A separate regression was performed for each survey. Water samples for Chl-*a* were collected from the ship's flowthrough seawater system at intervals during each voyage and matched to the geometric mean of Chl-*a* fluorescence calculated over ten-minute intervals, centred at the time of underway water sampling and fluorometric Chl-*a* measurement (2016: coef. = 0.28, int. = -0.93, n = 48, $R^2 = 0.85$, $p < 0.001$) or high-performance liquid chromatography estimate (HPLC; 2017: coef. = 1.09, int. = -2.69, n = 14, $R^2 = 0.97$, $p < 0.001$).

2.0. Tables

Table 1. The number of replicates used to calculate mean values for NASC across each polygon in the 2016 (n 2016) and 2017 (n 2017) surveys.

Polygon	n 2016	n 2017
N2.1	177	101
N2.2	181	55
N2.3	219	105
N1.1	170	146
N1.2	418	171
N1.3	221	66
S1.1	115	117
S1.2	243	130
S1.3	43	29
S2.1	200	127
S2.2	272	188
S2.3	236	170

Table 2. The four final GLMs generated through forward-stepwise AIC-based selection. Column names are as follows: df = residual degrees of freedom, Est = coefficient estimate, SE = standard error of the estimated coefficient, t = t-value. The original coefficient estimates test statistics are provided and the heteroskedasticity and autocorrelation consistent estimates (suffix: HAC) are also provided to indicate a more conservative test accounting for serial autocorrelation.

Model formula	df	Predictor	Est	SE	t	Pr(>|t|)		SE HAC	t HAC	Pr(>|t|) HAC	
NASC.2016 ~ bathymetry + temperature	2838	Intercept	-12.18	2.14	-5.69	< 0.001	***	2.77	-4.40	< 0.001	***
		bathymetry	0.05	0.00	15.24	< 0.001	***	0.01	9.82	< 0.001	***
		temperature	0.56	0.13	4.38	< 0.001	***	0.15	3.70	< 0.001	***
NASC.2017 ~ bathymetry + temperature	1569	Intercept	-2.28	0.89	-2.56	0.011	*	2.44	-0.93	0.350	.
		bathymetry	0.03	0.00	18.68	< 0.001	***	0.00	6.23	< 0.001	***
		temperature	0.34	0.06	5.57	< 0.001	***	0.17	2.01	0.044	*
NASC.2017 ~ bathymetry + temperature + log10(zooplankton biomass)	1075	Intercept	-6.94	1.17	-5.94	< 0.001	***	3.00	-2.31	0.021	*
		bathymetry	0.02	0.00	11.00	< 0.001	***	0.00	4.79	< 0.001	***
		temperature	0.72	0.09	7.69	< 0.001	***	0.23	3.08	0.002	**
		log10(zooplankton)	-0.24	0.14	-1.76	0.079	.	0.25	-0.96	0.335	.
Zooplankton Biomass ~ log10(chlorophyll) + bathymetry + temperature	682	Intercept	3.14	1.18	2.66	0.008	**	1.93	1.62	0.105	.
		log10(chl)	2.20	0.53	4.17	< 0.001	***	1.19	1.84	0.066	.
		bathymetry	-0.01	0.00	-5.18	< 0.001	***	0.00	-2.63	0.009	**
		temperature	0.42	0.08	4.95	< 0.001	***	0.14	2.90	0.004	**

3.0. Figures

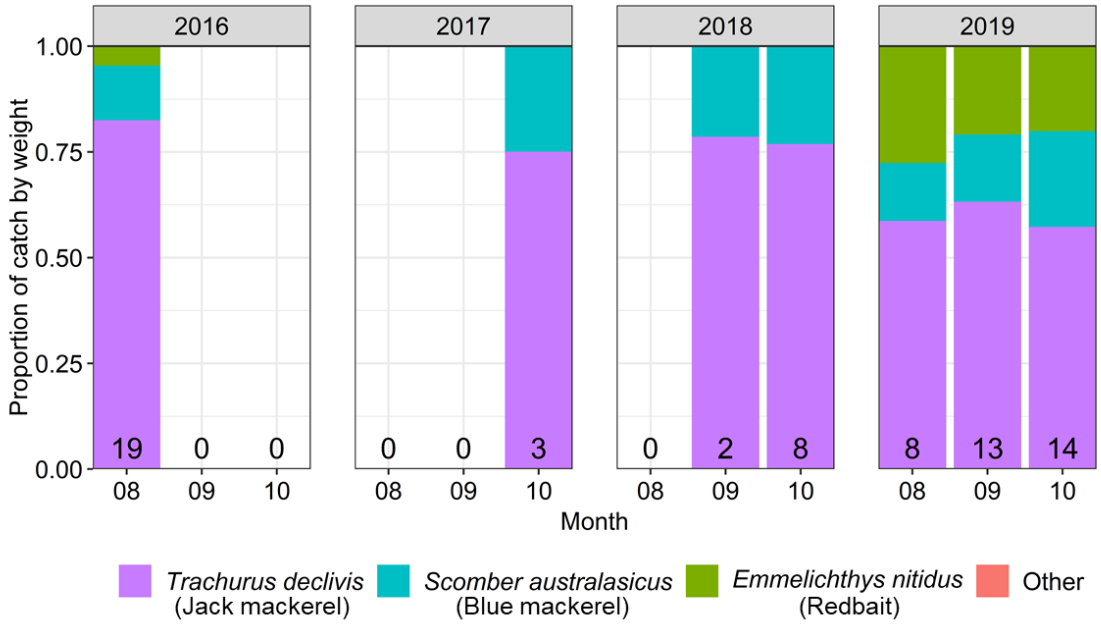

Fig. 1. Proportion of fisheries logbook catch by weight from midwater trawls in the Montague Island region for August to September 2016 to 2019. Numbers at the base of bars indicate the number of trawls used to calculate mean proportions. Missing bars indicate that fishing operations were not conducted in the region during the corresponding time period.

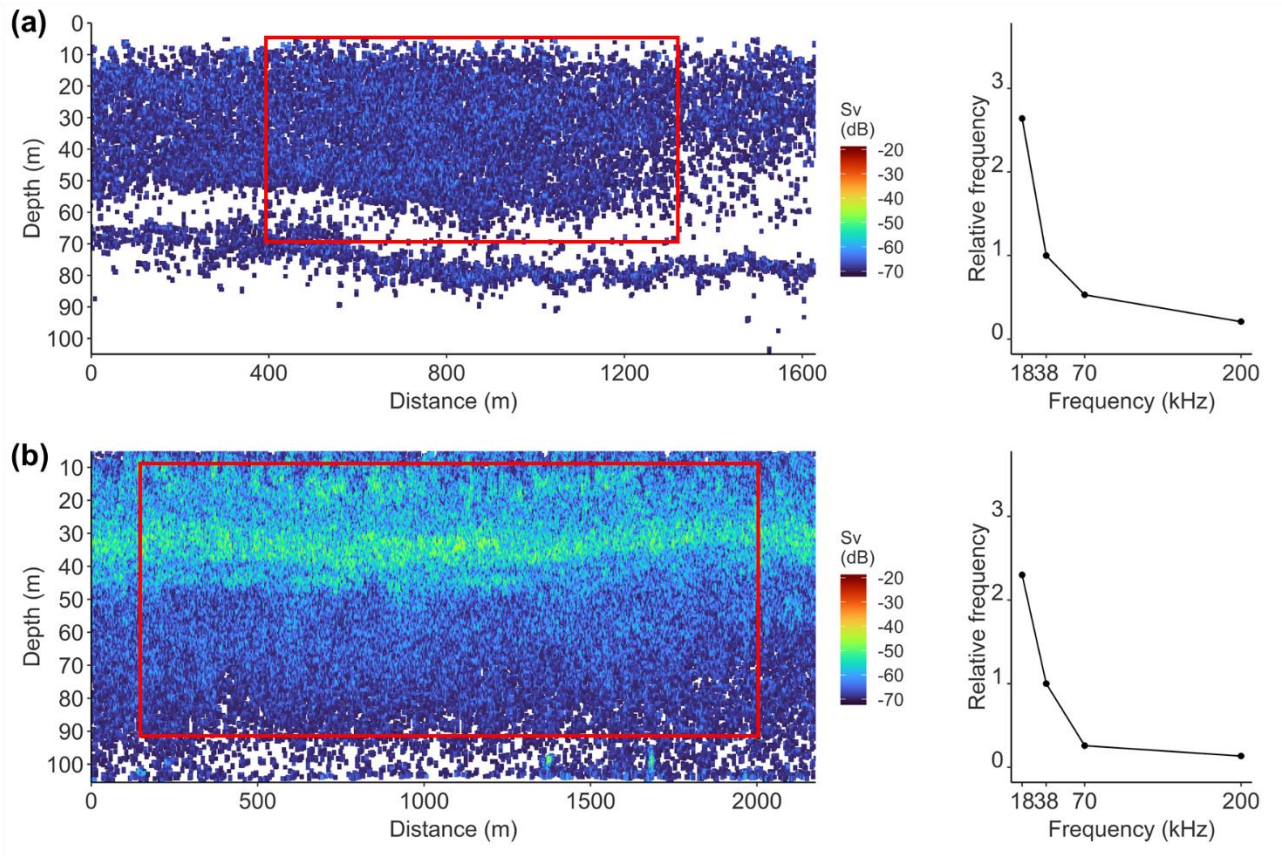

Fig. 2. A sample of echograms from the 2016 (a) and 2017 (b) surveys, along with relative frequency response plots (to the right of each corresponding echogram). Red boxes indicate the section of the echogram that was integrated to produce the relative frequency response plot.

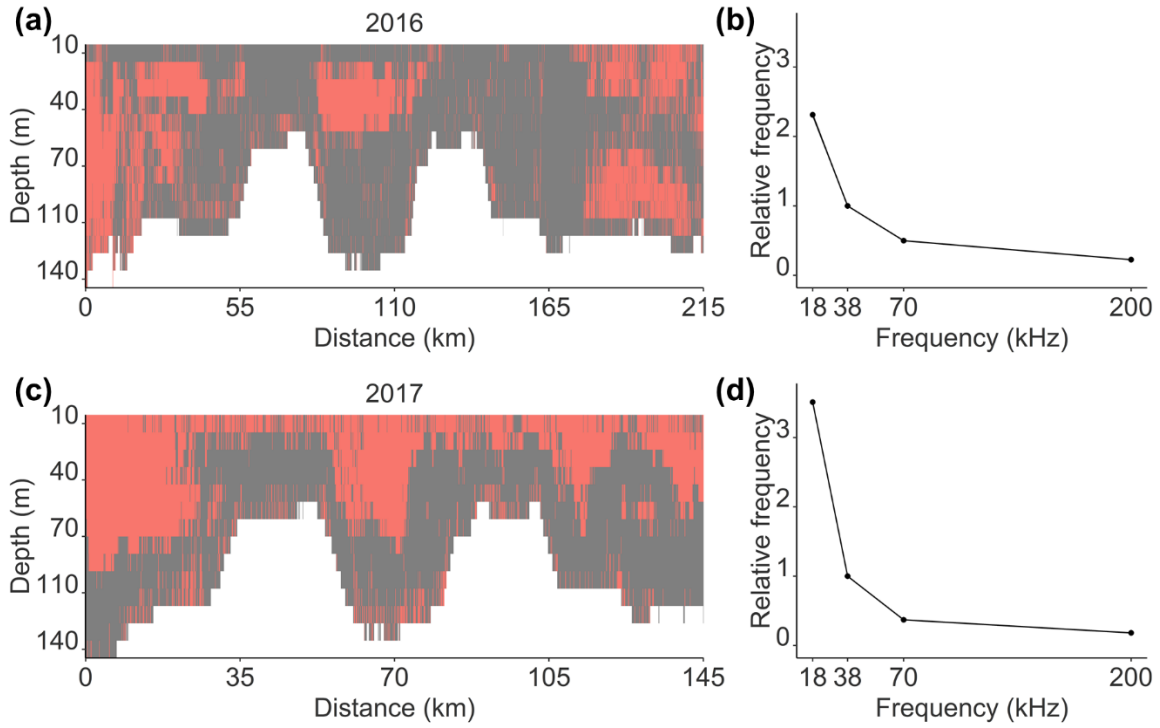

Fig. 3. Cells classified as fish for the 2016 (a) and the 2017 (c) surveys and the mean frequency responses (relative to S_{v38}) for cells which were classified as fish for the 2016 (b) and 2017 (d) surveys.

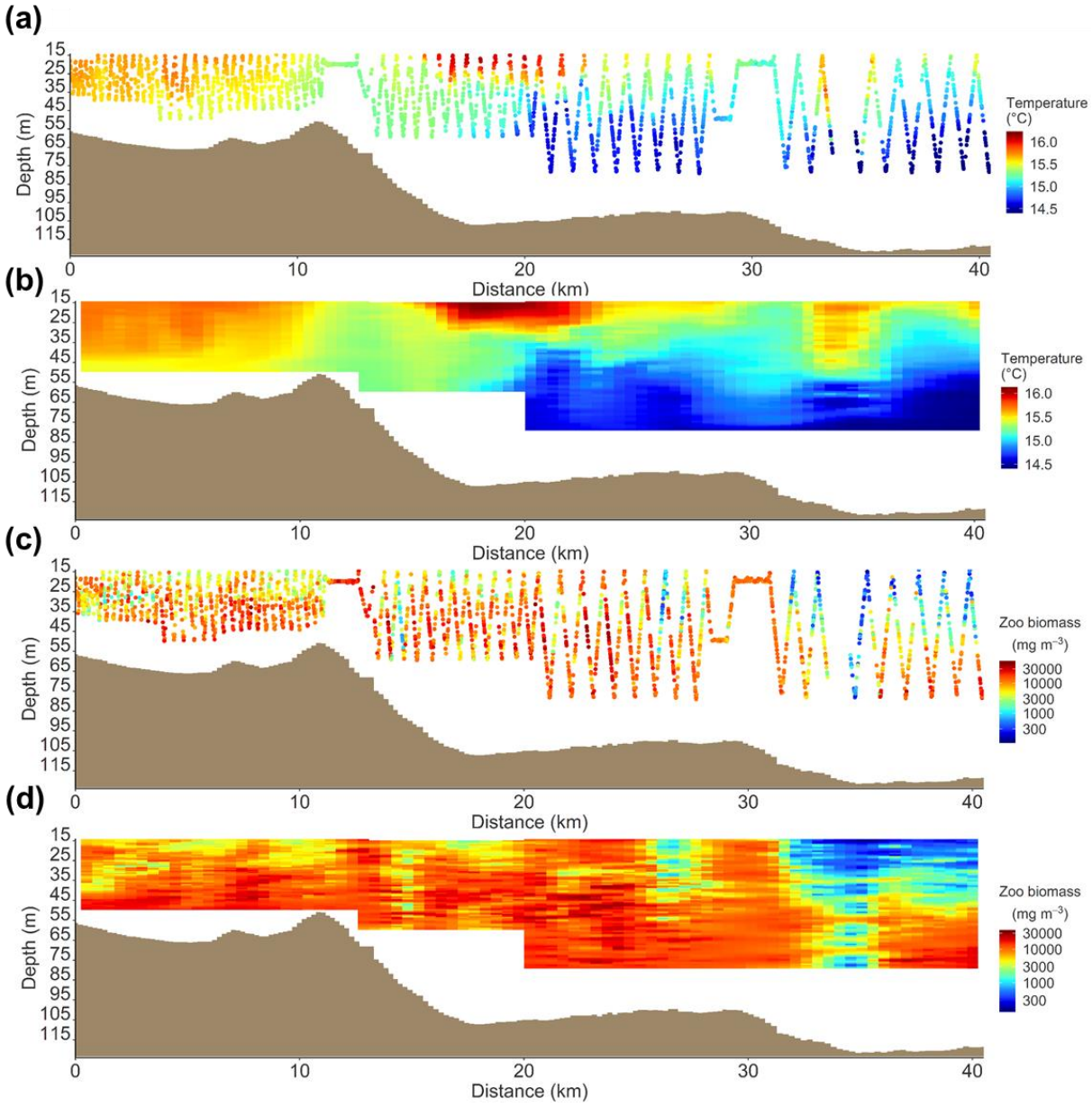

Fig. 4. Vertical profile of temperature (a) and zooplankton biomass (c) recorded by the undulating towed-body during the northern leg of the 2017 survey, and interpolated profiles generated using ordinary kriging of the raw temperature (b) and zooplankton biomass (d) data.

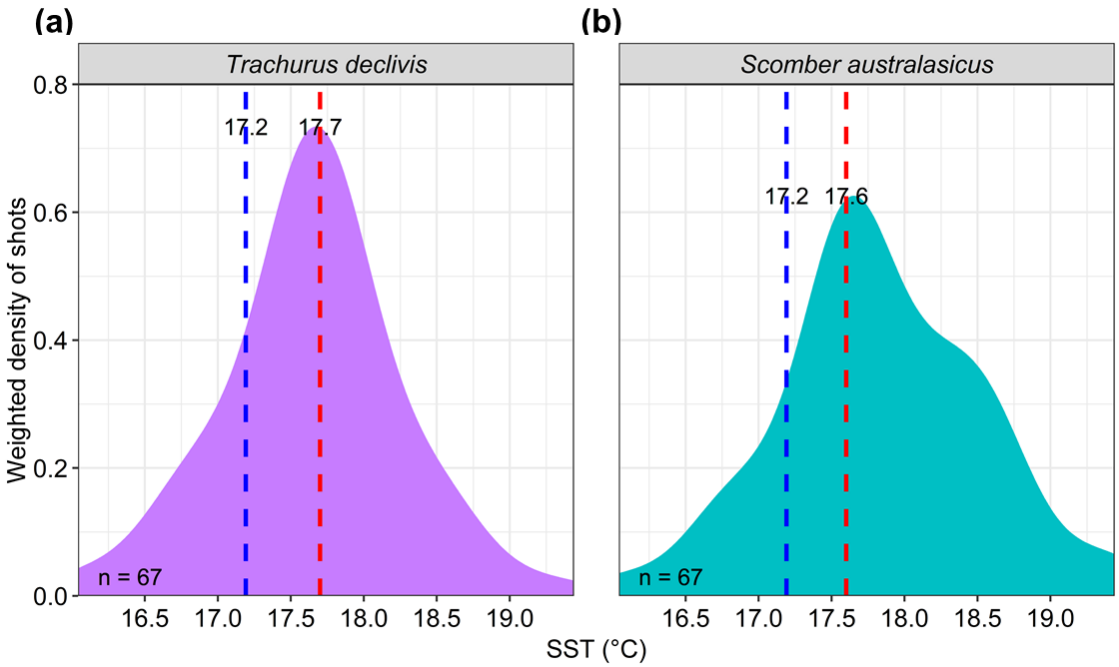

Fig. 5. Smoothed density estimates for the temperature distribution of commercial midwater trawls weighted by CPUE (kg hour^{-1}) for *Trachurus declivis* (a) and *Scomber australasicus* (b). The red vertical line indicates the peak in the temperature distribution for each panel and the blue line indicates the mean water temperature for the region (averaged between 100 to 200 m depth) for days when fishing operations occurred.

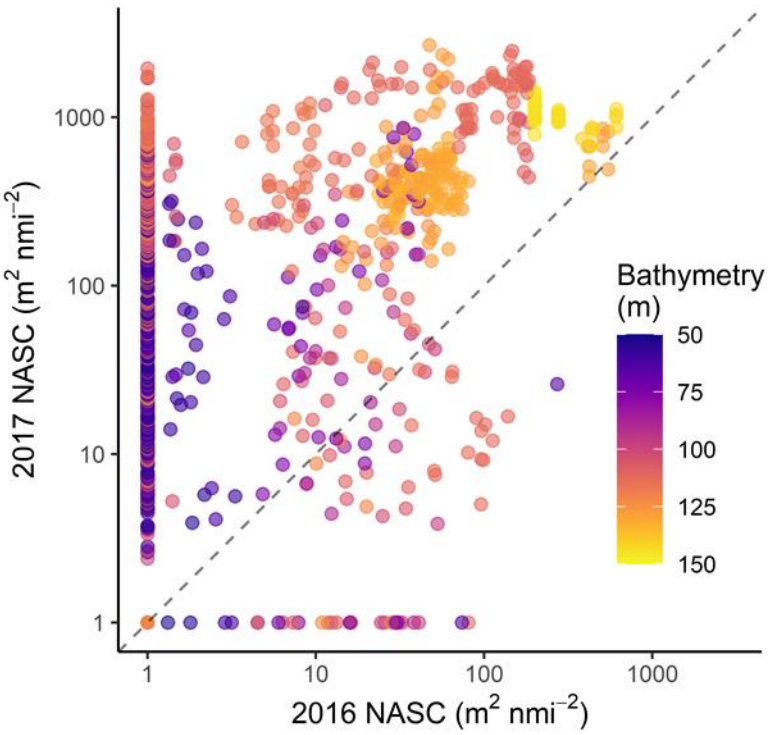

Fig. 6. Spatially paired NASC values for each of the 2016 and 2017 surveys (n = 1107, r = 0.40). Points are coloured by bathymetry. Points arranged in a linear pattern along the x-axis represent positive NASC values in 2016 with corresponding zero NASC in 2017 and vice versa for the y-axis.

Declaration of interests

☒ The authors declare that they have no known competing financial interests or personal relationships that could have appeared to influence the work reported in this paper.

☐The authors declare the following financial interests/personal relationships which may be considered as potential competing interests: